



## A 2600-year high-resolution climate record from Lake Trichonida (SW Greece)

Joana Seguin<sup>1</sup>, Pavlos Avramidis<sup>2</sup>, Walter Dörfler<sup>3</sup>, Alexandros Emmanouilidis<sup>2</sup>, and Ingmar Unkel<sup>1</sup>

<sup>1</sup>Institute for Ecosystem Research, Christian-Albrechts-Universität, Olshausenstraße 75, 24118 Kiel, Germany

<sup>2</sup>Department of Geology, University of Patras, Rio, 26504 Patras, Greece

<sup>3</sup>Institute of Pre- and Protohistoric Archaeology, Christian-Albrechts-Universität, Johanna-Mestorf-Straße 2–6, 24118 Kiel, Germany

**Correspondence:** Joana Seguin ([jseguin@ecology.uni-kiel.de](mailto:jseguin@ecology.uni-kiel.de))

**Relevant dates:** Received: 8 January 2020 – Revised: 30 June 2020 – Accepted: 28 July 2020 –  
Published: 8 October 2020

**How to cite:** Seguin, J., Avramidis, P., Dörfler, W., Emmanouilidis, A., and Unkel, I.: A 2600-year high-resolution climate record from Lake Trichonida (SW Greece), *E&G Quaternary Sci. J.*, 69, 139–160, <https://doi.org/10.5194/egqsj-69-139-2020>, 2020.

**Abstract:** This paper aims at reconstructing the palaeoclimatic changes during the last 2600 years in southern Greece based on a proxy record from Lake Trichonida. For the first time, we provide a reliable age-depth model and continuous geochemical data for the largest and deepest lake in Greece. We use X-ray fluorescence (XRF) geochemical data supported by discrete mineral analysis based on X-ray diffraction (XRD), grain size distribution, and organic matter content to investigate changes in the lake sedimentary system and identify the major forcing mechanisms. A principal component analysis based on the XRF geochemical composition identifies the variation between carbonate-rich material, precipitating predominantly under drier and/or warmer conditions, and terrigenous sediment input, with it being more prominent during wetter and/or colder conditions. The first principal component (PC1) shows a very strong correlation with the weathering proxy  $\log(\text{Rb}/\text{Sr})$ , and we interpret both proxies as depicting fluctuations in the hydrological conditions. A cluster analysis, conducted on the continuous geochemical and colour parameters, highlights the similarities in the sediment characteristics deposited during wetter phases, notably during 1850–1750, 1500–1400, ca. 1100, and ca. 100 cal BP.

When comparing the PC1 Trichonida record to independent records from the Balkans, we find generally concurring patterns on a multi-decadal to centennial scale. We show that phases with wetter conditions at Lake Trichonida coincide with a more negative North Atlantic Oscillation (NAO) index, suggesting that the precipitation variability in southern Greece is linked to changes in the NAO atmospheric pattern, as one major driving force. The 2600-year-long sedimentary record of Lake Trichonida contributes to a better understanding of Late Holocene palaeohydrological changes in an important climatic transitional zone in the eastern Mediterranean.

**Kurzfassung:** In diesem Artikel rekonstruieren wir paläoklimatische Veränderungen der vergangenen 2600 Jahre in Südgriechenland anhand von Proxies aus dem See Trichonida. Erstmals stellen wir ein verlässliches Alterstiefenmodell, sowie durchgängige, geochemische Daten für den größten griechis-

chen See zur Verfügung. Wir verwenden geochemische Daten aus Röntgenfluoreszenzanalyse (XRF), unterstützt durch diskrete Röntgen-Diffraktometrie (XRD), Korngrößenverteilungen und Messungen des Organikgehalts, um Änderungen im sedimentären System des Sees zu untersuchen und deren Haupteinflussfaktoren zu ermitteln. Mittels einer Hauptkomponentenanalyse der geochemischen Zusammensetzung, basierend auf den XRF Messungen, identifizieren wir als dominierenden Prozess die Schwankungen zwischen Carbonaten auf der einen Seite, welche vorrangig während trockener und/oder wärmerer Bedingungen ausfallen, und terrigenem Material auf der anderen Seite, welches insbesondere in feuchteren und/oder kühleren Phasen eingetragen wird. Wir interpretieren diese Schwankungen als Änderungen in den hydrologischen Gegebenheiten. Ein Vergleich der ersten Hauptkomponente (PC1) mit dem Verwitterungsproxy  $\log(\text{Rb}/\text{Sr})$  weist hohe Übereinstimmungen auf, und wir interpretieren beide als Proxies für Schwankungen in den hydrologischen Gegebenheiten. Eine Clusteranalyse, basierend auf den kontinuierlichen geochemischen sowie Farbwerten, verdeutlicht die Ähnlichkeiten in den Eigenschaften der Sedimente, welche während feuchterer Phasen abgelagert wurden, insbesondere in den Zeiträumen 1850–1750, 1500–1400, ca. 1100 und ca. 100 cal BP.

Der Vergleich des PC1 Trichonida Datensatzes mit unabhängigen Proxies anderer Studien aus der Balkanregion zeigt grundsätzlich übereinstimmende Muster auf multidekadischen bis hundertjährigen Zeitskalen. Wir zeigen, dass Phasen mit feuchteren Bedingungen im Einzugsgebiet des Sees Trichonida mit einem negativen Index der Nordatlantischen Oszillation (NAO) zusammenfallen, woraus sich schließen lässt, dass die Niederschlagsvariabilität in Südgriechenland zu einem Großteil von Veränderungen im Muster der NAO geprägt ist. Der 2600 Jahre abdeckende Sedimentkern aus dem See Trichonida trägt zu einem besseren Verständnis natürlicher, spätholozäner paläohydrologischer Schwankungen in einer klimatisch wichtigen Übergangszone im östlichen Mittelmeer bei.

## 1 Introduction

Climatic changes and anthropogenic land use are two of the most significant driving forces of hydrological and geomorphological processes. As the interaction and connectivity between humans, climate, and environment are complex, it is necessary – though challenging – to differentiate anthropogenic from climatic impacts on landscape development over long timescales. Due to the long history of human–environment interaction in the Mediterranean, the region is especially valuable for interdisciplinary studies on past climate variability and human activity (McCormick et al., 2012; Mercuri and Sadori, 2014; Roberts et al., 2011; Weiberg et al., 2016).

Greece is located in a transitional zone between the temperate climate and the Mediterranean climate. Different large-scale atmospheric circulation patterns influence the Greek and eastern Mediterranean climate, such as the North Atlantic Oscillation (NAO), the Siberian High pressure system, and the East Atlantic/West Russia (EA/WR) pattern, mainly in winter, as well as the South Asian monsoon in summer (Barnston and Livezey, 1987; Xoplaki et al., 2003b, a). However, the rugged topography with its strong relief gradients and different mountain ranges acting as orographic boundaries lead to quite a heterogeneous modulation of these large-scale teleconnection patterns on a local level, influencing for example the amount of mean annual precipitation (Koutsodendris et al., 2017; Xoplaki et al., 2003a).

In southern Greece, high-resolution environmental archives completely covering the last 2600 years have been relatively sparse, have been often incomplete, or present divergent results (Finné et al., 2011, 2019; Katrantsiotis et al., 2019; Luterbacher et al., 2012), but the number of studies has been increasing recently (Emmanouilidis et al., 2018, 2019; Katrantsiotis et al., 2018, 2019; Seguin et al., 2019, 2020a). For the last 2600 years, a couple of major climatic phases and events have been identified for different regions across Europe, such as the Roman Warm Period (RWP, ca. 2200–1550 BP; Luterbacher et al., 2016; McCormick et al., 2012; Morellón et al., 2016; Wilson et al., 2016), the Late Antique Little Ice Age or Migration Period (LALIA, ca. 1400–1600 BP; Büntgen et al., 2016; Helama et al., 2017), the Medieval Climate Anomaly (MCA, ca. 1000–700 BP; Christiansen and Ljungqvist, 2017; Keigwin, 1996; Mangini et al., 2005), and the Little Ice Age (LIA, ca. 700–100 BP; Christiansen and Ljungqvist, 2017; Keigwin, 1996; Kelly and Ó Grada, 2014). It seems however that their manifestations were spatially and temporally very different (Neukom et al., 2019), and local studies are needed to investigate the partly diverging characteristics.

In this article, we present a new sedimentological archive from Lake Trichonida, the largest Greek lake. Our aims are (1) to obtain a solid age-depth model, (2) to compile high-resolution geochemical records for palaeoclimatic reconstructions from Lake Trichonida, and (3) to study climatic trends in southern Greece and investigate major forc-

ing mechanisms during the Late Holocene by comparing our results with independent palaeoclimate studies from the Balkans and the eastern Mediterranean.

## 2 Regional setting

Lake Trichonida (Λίμνη Τριχωνίδα, or in old Greek *Trichonis*) (38.56° N, 21.55° E) is the deepest and largest natural lake in Greece, located in the region Aetolia-Acarmania (Fig. 1). The lake is up to 19 km long and 6 km wide, stretching approx. in W–E direction and covering approx. 97 km<sup>2</sup>; it has a maximum depth of 58 m and a mean depth of 30.5 m. (Tafas et al., 1997). Inter-annual water level fluctuation in the lake is about 1 m (Tafas et al., 1997).

The lake has been studied irregularly since the 1970s with a focus on different limnological or biological aspects (Albrecht et al., 2009; Bottema, 1982; Creer et al., 1981; Koussouris and Diapoulis, 1982; Krüger and Damrath, 2020; Tafas et al., 1997; Zacharias and Ferentinos, 1997; Zotos et al., 2006; and references herein).

According to the Köppen classification, the lake is located in a Csa climate zone, indicating a temperate climate with hot and dry summers and mild and humid winters (coldest month mean temperature > 10 °C, warmest month mean temperature > 22 °C; rainfall during dry period < 30 mm) (Köppen, 1936; Tafas et al., 1997). According to Koussouris and Diapoulis (1982) the area is dominated by westerly winds. Precipitation, which mainly falls in winter (Fig. 2), is controlled by eastbound cyclones originating from the Atlantic (Finné et al., 2011; Xoplaki et al., 2003a).

Lake Trichonida is situated in the Trichonis graben, a highly tectonized and complex hydrogeological system (Albrecht et al., 2009; Kiratzi et al., 2008). While the mountains surrounding the lake rise up to 2000 m a.s.l., the lake itself lies in the Agrinio depression at approx. 10 m a.s.l. The Pindos thrust cuts right through the lake and a normal fault, striking E–W and dipping north, bounds the southern flank of the lake (Overbeck et al., 1982).

The size of the lake catchment varies according to the sources between 215 and 421 km<sup>2</sup> (Dimitriou and Zacharias, 2006; Overbeck et al., 1982; Zacharias et al., 2002). It mainly consists of highly tectonized, karstified calcareous rocks in the NE (Fig. 1), where groundwater inflow is of high importance; impermeable flysch formations in the SW; and Quaternary sediments in the direct vicinity of the lake (Dimitriou and Zacharias, 2006; Overbeck et al., 1982; Tafas et al., 1997). Thirty seasonal streams discharge into the lake (Dimitriou and Zacharias, 2006). Lake Trichonida drains into the smaller, neighbouring Lake Lysimachia in the west through a controlled outflow canal (Avramidis et al., 2013; Dimitriou and Zacharias, 2006) and further into the river Acheloos (Overbeck et al., 1982). The lake's water balance is presented by Overbeck et al. (1982). Lake Trichonida is a warm, monomictic lake that is stratified during summer and mixes in

winter (Tafas et al., 1997). During summer months the thermocline lies between 14 and 26 m (Overbeck et al., 1982). With respect to its nutrient balance, Tafas et al. (1997) describe it as oligotrophic with mesotrophic tendencies. This is in good agreement with the low amount of chlorophyll *a* (2.3 mg m<sup>-3</sup>) reported by Zacharias et al. (2002), which indicates a low algal growth in the water body. Albrecht et al. (2009) found a high number of endemic molluscs in the lake, and Tafas and Economou-Amilli (1997) studied seasonal phytoplankton assemblages and also report endemic diatoms.

The catchment area is covered by pine, fir, oak, and Greek maquis shrubland (Koussouris and Diapoulis, 1982). The flat shore area is intensively used for agricultural purposes. For present aquatic vegetation refer to Koussouris and Diapoulis (1982). A pollen study by Bottema (1982) provides some indication on vegetation transformation during the Late Holocene. The continuous presence of anthropogenic indicators (e.g. viticulture) indicates human influence upon the vegetation in the area for the complete investigated period. Nowadays, the lake area is part of the Natura 2000 environmental protection network as a habitats directive site, as it conserves endangered or protected flora and fauna and serves as a resting area for migratory water birds (European Environment Agency, 2020; Dimitriou and Zacharias, 2006).

## 3 Material and methods

### 3.1 Fieldwork

Fieldwork was conducted in spring 2018 using a Usinger piston corer system (Mingram et al., 2007), newly modified with a wire-operated second platform at the lake bottom. The coring site TRI1 is located in the deepest central eastern part of the lake (38°33'0.61" N, 21°35'20.76" E; 50 m water depth). We recovered two overlapping parallel cores with 80 mm diameter in the upper part and 55 mm diameter in the lower part and retrieved them in 2 m sections. Offset between the cores was 50 cm (see Table S1 in the Supplement). The sediment cores were removed from the coring equipment, cut into 1 m sections for better handling, split open longitudinally on site, and transferred into plastic U channels that were thoroughly labelled and sealed. At Kiel University (Germany), they are stored at +4 °C in a cooling container for further processing.

### 3.2 Dating

The chronology of the Trichonida sediment sequence is based on 13 accelerator mass spectrometry (AMS) radiocarbon (<sup>14</sup>C) dates, processed at the Poznań Radiocarbon Laboratory (Table 1). Radiocarbon dating was performed on two groups of samples: organic macro-remains and bulk sediment samples, in the case of absence of visible macro-remains. Where visible, macroscopic plant remains were extracted from the sediment cores, isolated under a reflected

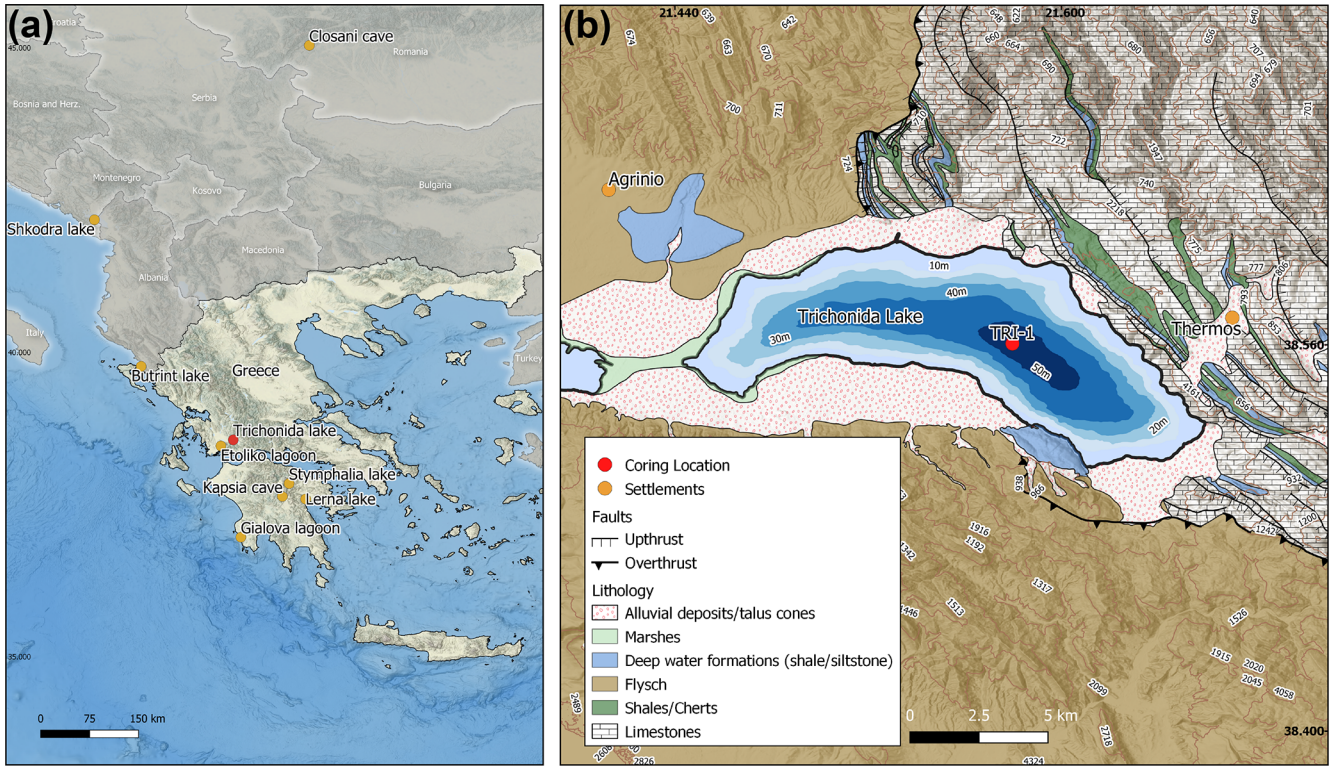


**Figure 1.** Map of the study area. (a) Overview map of Greece and the Balkans. Lake Trichonida is marked in red. Key sites used for comparison in Fig. 8 are indicated in yellow. (b) Map showing the study area with the coring site, the topography, and geology. Agrinio as the largest city and Thermos as the most important archaeological site are indicated. The map was created using QGIS. The geological map is based on IGME (1988, 1977).

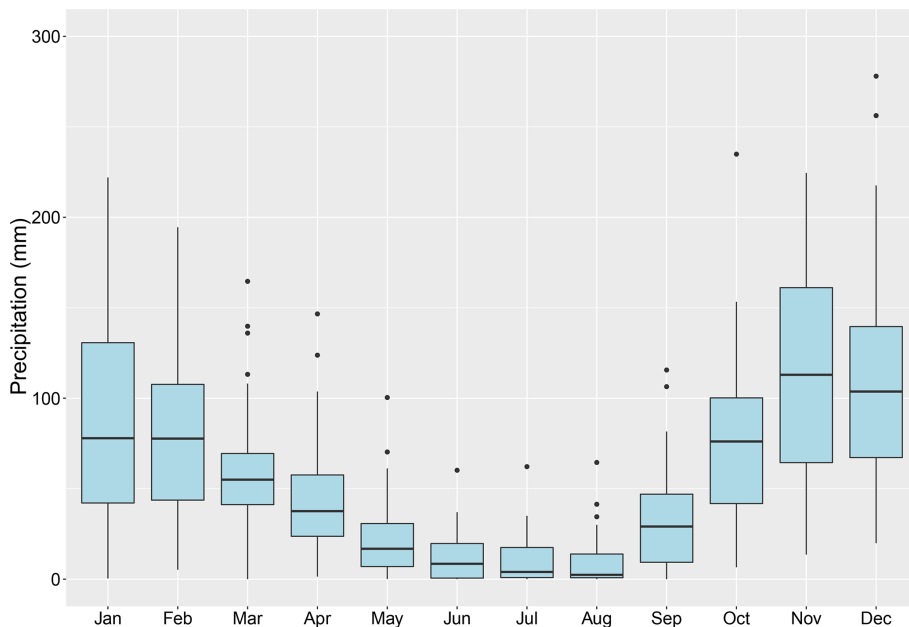


**Figure 2.** Mean monthly precipitation for Araxos. The mean monthly precipitation from January to December for the WMO station Araxos Airport (38.133° N, 21.416° E) is shown for the period 1961–1990.

light binocular, and rinsed with deionized water. They consisted of charcoal or plant remains, twigs, or leaves (Table 1). In the lower part of the cores, where no macro-remains could be found, we used bulk sediment samples for  $^{14}\text{C}$  dating (Fig. S1).

The age-depth modelling was done using *rbacon* (Blaauw and Christeny, 2011; Fig. 5). All dates are indicated as calibrated calendar years before present (calBP), where “present” is defined as 1950 CE with  $1\sigma$  uncertainty ranges following Mook and van der Plicht (1999). Mean ages were extracted from the model and used for the representation and interpretation of the proxy data.

### 3.3 Analytical methods

The cores were described concentrating on lithology, sediment texture, and structure as well as on sediment colour according to Munsell soil colour charts (Munsell, 2000) and macroscopic remains. The core sections were visually correlated on distinct marker layers that were used as tie points where possible and fine-tuning was done in a second step based on the RGB (red, green, blue) colour values and XRF scans.

The surfaces of the half cores were smoothed and photographed using a digital line-scan camera (resolution:  $143\text{ pixels cm}^{-1}$ ). Based on RGB values and  $L^*a^*b^*$  ( $L^*$  for lightness,  $a^*$  from green to red, and  $b^*$  from blue to yellow) from the CIELAB colour space, colour profiles were created to depict colour variations with depth (Fig. 3).

The cores were scanned for XRF using an Avaatech core scanner with a rhodium X-ray source. The scanning settings were a 1 mm resolution at 10 kV (exposure time of 10 s at 250  $\mu\text{A}$ ) and at 30 kV (exposure time of 10 s at 1000  $\mu\text{A}$  using a Pd-thick filter). The XRF scans provide semi-quantitative element intensities in total counts per second (tcps). Eleven elements (10 kV: Al, Si, K, Ca, Ti, Mn, Fe, Co; 30 kV: Rb, Sr, Zr) show continuous data for 438 cm of TRI1 and are used for further analysis. We analyse relative changes of one element to another by natural logarithmic (log) ratios and interpret these as proxies for palaeoenvironmental variation. Hence, measurement variation caused by sample geometry, physical properties, water content, and the closed-sum effect are minimized (Tjallingii et al., 2007; Weltje and Tjallingii, 2008).

Twenty-four samples, at least one per lithological unit (Fig. 4), were analysed for their grain size distribution (GSD) using a laser particle analyser, Malvern Mastersizer 2000. The 70 measured classes were grouped into the seven common grain size fractions following the ad-hoc Arbeitsgruppe Boden (2005).

Mineralogical analysis was conducted on 15 representative samples from different lithological units using X-ray diffraction (XRD, Bruker D8 Advance). Determination and qualitative analysis of the results were performed through DIFFRACplus EVA12 software (Bruker AXS), by calculation of the area method, characterizing the method as semi-

quantitative. The full width at half maximum (FWHM) of each diagnostic peak was measured for each detected mineral percentage to be calculated. The minimum detection limit is around 2 %–3 %, with small variations depending on the state of the studied sample.

Carbon and nitrogen samples were taken at approximately 25 cm resolution. The concentrations of total carbon (TC), total inorganic carbon (TIC), and total nitrogen (TN) were determined on dried, powdered, and homogenized samples, using a Euro EA elemental analyser. Total organic carbon (TOC) was calculated from the difference between TC and TIC. The TOC/TN ratio was calculated to indicate the origin of the sedimentary organic matter. While values for in-lake organic matter, such as algae, are low, generally ranging between 4 and 10, mixed provenance is indicated by a ratio of 10 to 20; values higher than 20 indicate that land-plant organic matter was eroded into the lake (Meyers, 2003).

All statistical analyses, diagrams, and figures were compiled using the software R version 3.6.1 (R Core Team, 2019). For the RGB and XRF data, cleaning of the datasets, i.e. the removal of explicit outliers due to unevenness or cracks in the sediment core and the refilling of the missing values by linear interpolation, was done prior to statistical processing.

In this study, Spearman’s correlation coefficient (Spearman, 1904) was employed to examine correlations between two populations. We conducted a principal component analysis using the *prcomp* function from the R stats package on the centred log-transformed XRF dataset. A hierarchical cluster analysis was performed on the centred log-transformed XRF data and the continuous RGB colour parameters with *hclust* from the R stats package, using Euclidean distances as the distance measure and complete linkage as the agglomeration method.

## 4 Results

### 4.1 Core description

Based on the composition, structure, and colour, the investigated core sequence of TRI1 was divided into 15 lithological units and subunits (Figs. 3, 4, Table 2).

The core dominantly consists of homogeneous, non-laminated marls of greyish colour. While few plant macrofossils were found, carbonate macrofossils are completely absent. The sediment sequence does not show any signs of annual lamination or blackish mud, including high organic matter content, although the lake is classified as monomictic, implying a turnover only once a year and a vertical stratification of the water body throughout most of the year. The X-ray diffraction (XRD) analysis indicates that the most prominent mineral phase throughout the core consists of clay minerals (25.2 %–53.1 %), followed by chlorite (15.6 %–41.0 %), calcite (4.9 %–41.2 %), and quartz (9.2 %–25.3 %; Fig. S4); other minerals were absent or below the detection limit.

**Table 1.** List of all radiocarbon samples taken from TRI1. Indicated  $^{14}\text{C}$  ages are unmodelled ages giving the 68.2 % calendar dating probability. Calibrated ages are cal BP ages using the IntCal13 calibration dataset (Reimer et al., 2013).

Sample no.	Analysis no.	Sample material	C content in this fraction <sup>a</sup> (mg C)	$^{14}\text{C}$ age $\pm 1\sigma$ (BP)	Calibrated $^{14}\text{C}$ age (cal BP), $1\sigma$ ranges	depth (cm)
TRI-res01	Poz-106295	terrestrial plant for reservoir age	0.5	$0 \pm 30$	236–235 59–42	0 <sup>b</sup>
TRI-65	Poz-105729	twig		$175 \pm 30$	282–267 215–168 153–144 20–0	65
TRI-183	Poz-106296	leaf of deciduous tree	0.7	$1150 \pm 30$	1171–1161 1121–1112 1085–1046 1033–984	183
TRI-219	Poz-110650	leaf of deciduous tree		$1320 \pm 30$	1292–1257 1202–1188	219
TRI-229	Poz-105452	drupe		$2605 \pm 35$	2758–2730	229 <sup>b</sup>
TRI-299	Poz-110652	bulk sediment		$3605 \pm 30$	3966–3944 3930–3871	299 <sup>b</sup>
TRI-310	Poz-106297	charcoal		$1940 \pm 30$	1926–1865 1840–1835	310
TRI-375	Poz-110651	charred plant remains		$2190 \pm 30$	2304–2237 2182–2148	375
TRI-461	Poz-105390	charred plant remains		$2640 \pm 35$	2774–2745	461
TRI-490	Poz-110653	bulk sediment		$9290 \pm 50$	10 567–10 416	490 <sup>b</sup>
TRI-532	Poz-110654	bulk sediment	0.8	$8210 \pm 40$	9257–9117 9104–9093	532 <sup>b</sup>
TRI-559	Poz-106298	bulk sediment	0.8	$9080 \pm 50$	10 257–10 198	559 <sup>b</sup>
TRI-598	Poz-100656	bulk sediment		$8410 \pm 50$	9493–9404 9340–9332	598 <sup>b</sup>
TRI-627	Poz-106299	bulk sediment	0.8	$10440 \pm 60$	12 522–12 471 12 430–12 372 12 352–12 232 12 207–12 167	627 <sup>b</sup>

<sup>a</sup> Amount of remaining sample material after respective pretreatment if  $< 1.0$  mg C. <sup>b</sup> Excluded from the final age-depth model.

Changes in lithology are closely related with changes in colour parameters (RGB and  $L^*$ ,  $a^*$ ,  $b^*$ ). Contrary to the RGB values, the  $a^*$  parameter, spanning from green to red, and the  $b^*$  parameter, spanning from blue to yellow, allow a differentiation of the thin, blueish and reddish sedimentary units. Towards the top, the amount of yellow colour particles is steadily increasing (Fig. 3). This is interrupted by thin layers of very different colouration. Units 11, 12, and 14 have a reddish colour, while units 16 and 18 depict a dark-grey to blueish colour, more intense than unit 9, as visible in the  $a^*$  colour proxy (Fig. 3).

The grain size distribution is very uniform and clearly dominated by silt-sized material; sediment types can be distinguished ranging from clayey to very clayey silt. Clay content varies from 11.95 % to 21.74 %, and the sand fraction is hardly present with only 0 % to 4.36 %. A large share of the silt-sized particles is of calcareous origin as can be expected due to the limestone geology of the catchment (Fig. 4).

The TOC content ranges between 1.2 % and 2.3 %, with the TOC/TN ratio being in the range 15.5–48.6, indicating a predominantly to exclusively terrestrial source and allochthonous origin of the organic matter.

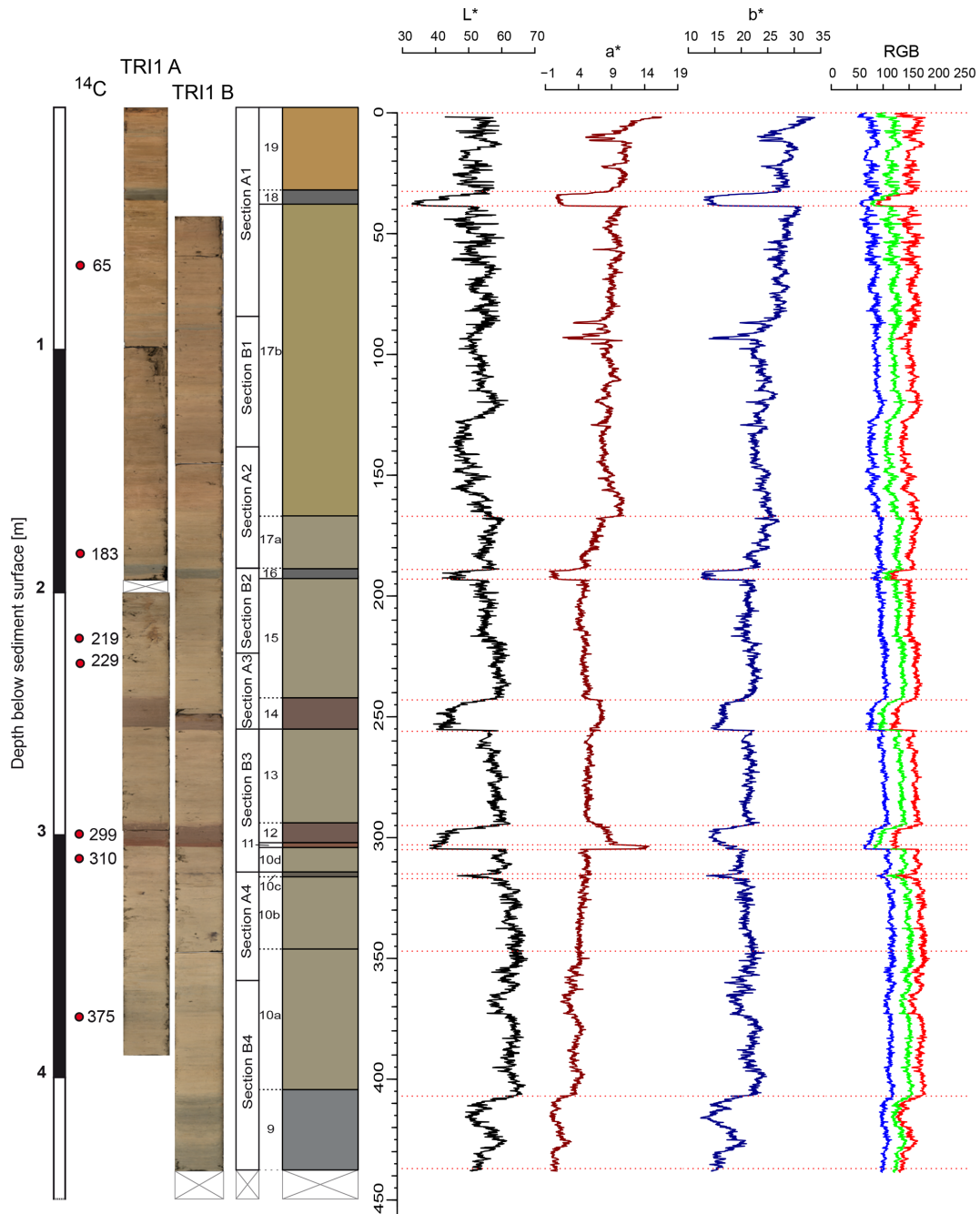


**Figure 3.** Core pictures of TR11-A and TR11-B and lithological profile of the master core TR11 are plotted against depth. The composite sections and the delimited lithological units are indicated. Depths where samples for  $^{14}\text{C}$  dating were taken are marked by red dots. On the right panel, colour sequences in  $L^*a^*b^*$  and RGB colour code are depicted.

The three independent indicators of calcium carbonate, XRF Ca, TIC, and XRD calcite, are generally in good agreement (Fig. 4). Carbonate content (Ca and Sr) strongly varies along the sequence and is lowest in the blueish and reddish sedimentary units (11, 12, 14, 16, and 18; Fig. 4). Quartz content shows only minor variation but a distinct maximum in unit 11. Together with several terrigenous elements (Rb, K,

Zr), Sr shows an exceptionally high peak in unit 10c, which was addressed as a tephra layer (see Sect. 5.1). Besides, Sr and Ca show a high correlation ( $r_{\text{Spearman}} = 0.88$ ) and a similar curve progression with depth (Fig. 4).

The terrigenous elements (Ti, Rb, Fe, Zr, K, Al, and Si) all show a very similar behaviour along the entire sediment

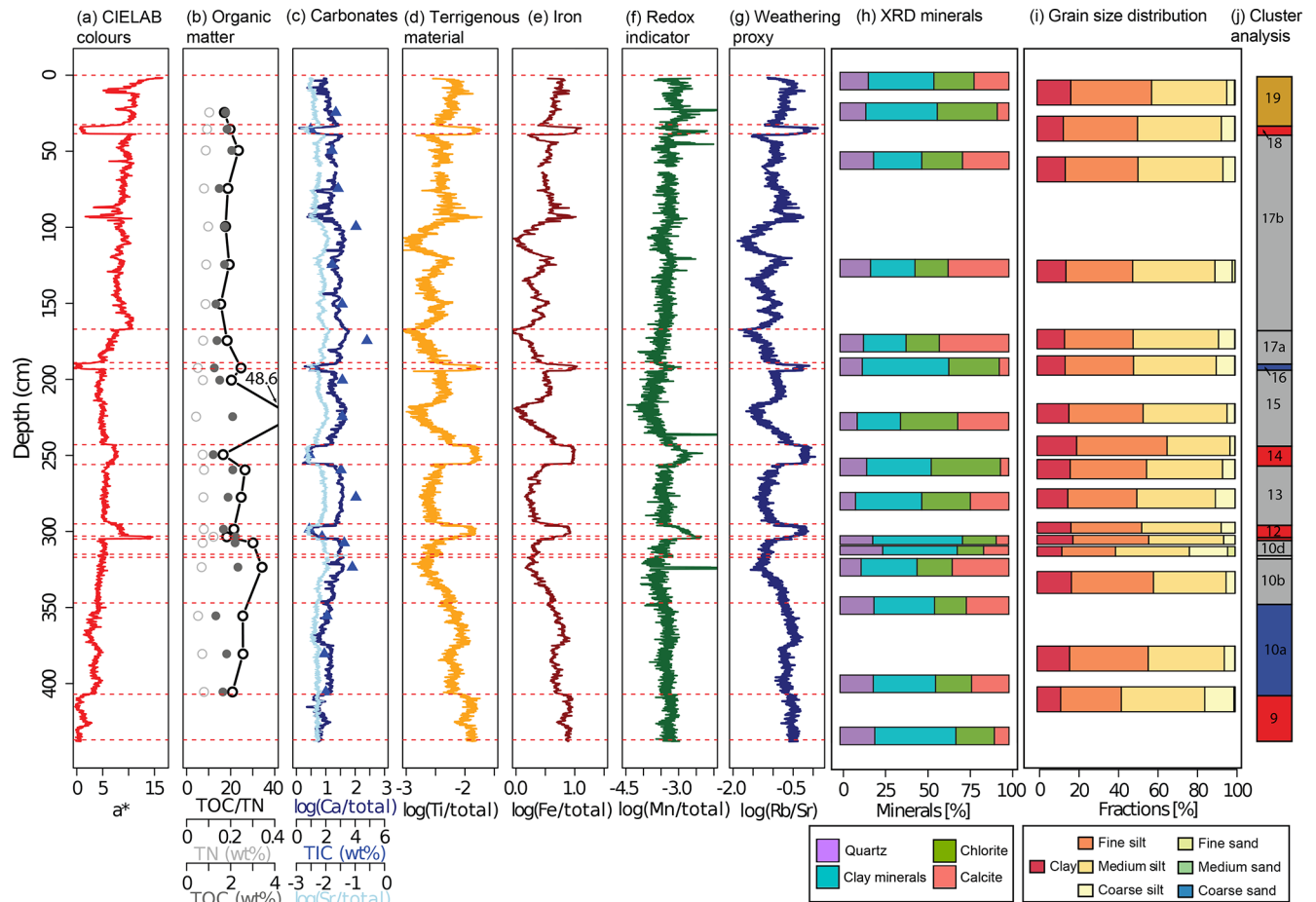


**Figure 4.** Overview of selected colour, organic, and geochemical proxies for the composite profile TRI1 plotted against depth. **(a)** CIELAB colour parameter  $a^*$ , **(b)** organic matter proxies (TOC, filled points; TN, empty points; and C/N, points on line), **(c)** carbonate proxies (Ca, blue line; Sr, bright blue line; and TIC, triangles), **(d)** terrigenous material (Ti), **(e)** iron (Fe), **(f)** redox indicator (Mn), **(g)**  $\log(\text{Rb}/\text{Sr})$  as weathering proxy, **(h)** XRD minerals, and **(i)** discrete grain size measurements. Bar widths for XRD and grain size distribution are not at scale. **(j)** The lithological units; colour coding follows the cluster analysis. All XRF elements presented here have been normalized against total counts and log transformed. Horizontal, red dashed lines indicate lithological units.

sequence. The highest values occur in the thin blueish and reddish sedimentary units and in the lowermost unit 9.

Manganese (Mn) values are rather constant along the core with increasing variance only in the uppermost unit 19. In the thin units 11, 12, 14, and 18, Mn shows enhanced values at the bottom of the unit with a decreasing trend towards the top (Fig. 4). The  $\log(\text{Rb}/\text{Sr})$  ratio shows irregular cyclic variation with depth, with higher values in the blueish and reddish sedimentary units and below 350 cm (Fig. 4).

#### 4.2 Age-depth model

Due to the limestone-rich environment, there is a high amount of reworked, inorganic carbon present in the sediment, which may lead to too old  $^{14}\text{C}$  ages when dating bulk sediment (Grootes et al., 2004; Seguin et al., 2019). Six macro-remain-based radiocarbon ages form the basis of the final, most reliable age-depth model. To obtain a higher reliability,

the model was cut at the lowermost date obtained from organic remains (461 cm), corresponding to an approximate basal age of 2750 cal BP. All bulk sediment samples were finally excluded from the age-depth model, as they yielded considerably too old ages (see Fig. S1). This was best visible when comparing the bulk sediment age at 299 cm with the charcoal sample at 310 cm; these two dates are only 11 cm apart but depict an age difference of 1700 years. We took a surface sample from aquatic plants (TRI-res01) to analyse for a potential hard water effect or reservoir age, but this sample yielded a recent  $^{14}\text{C}$  age, suggesting that the lake is not affected by reservoir effects at least under current conditions. Dating challenges due to the low preservation of organic material, hard water, and old carbon effects due to the limestone bedrock are known for Greek lakes (Bottema, 1982; Seguin et al., 2019; Vaezi et al., 2019). However, a critical assessment of the dating results and an extensive modelling

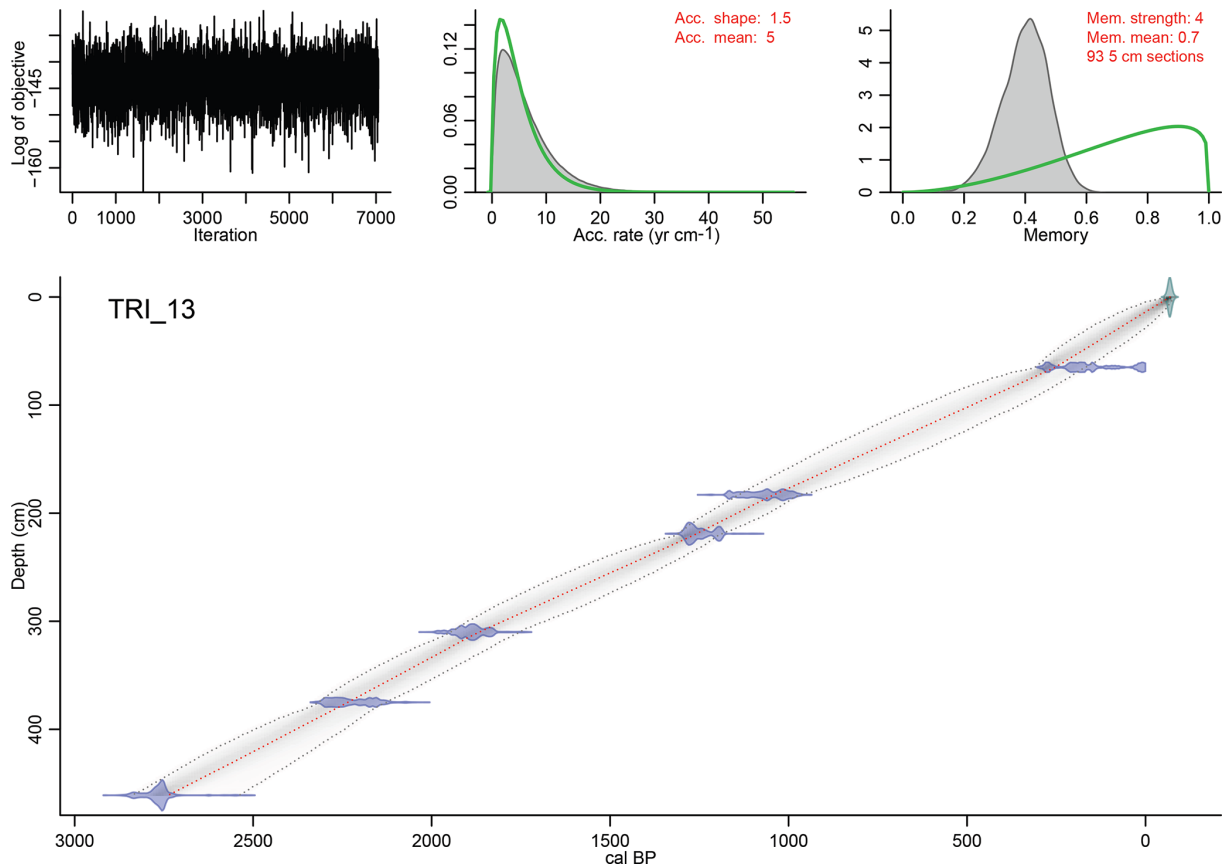


**Figure 5.** Bayesian age-depth model TRI\_13 constructed using the R package rbacon (Blaauw and Christen, 2011). The blue tie bars indicate the  $^{14}\text{C}$  age distribution, while the greyscale of the line graph reflects the likelihood; the dotted red line follows the mean ages.

approach, if possible, combined with other numeric or relative age information, still yields a solid and reliable age-depth model. The final model shows a continuous and rather constant sedimentation rate of  $1.68 \text{ mm yr}^{-1}$  over the investigated period.

### 4.3 Statistical analyses of the geochemical data

#### 4.3.1 Cluster analysis

A hierarchical cluster analysis was conducted on the continuous XRF and  $L^*a^*b^*$  proxies (14 variables) to independently classify the 15 visually determined lithological units and subunits according to potentially different sedimentary conditions (Fig. 6).

Our clusters show meaningful correlations with the sedimentological units. The results allow a differentiation into two sound main clusters and five systematically traceable sub-clusters, and the results are depicted in a dendrogram (Fig. 6). Four main lithofacies may be distinguished, leaving aside the tephra (unit 10c, see Sect. 5.1), suggesting rather similar environmental conditions during the deposition of material within the same sub-cluster.

Cluster 1 comprises unit 10a and the thin unit 16, which cover the periods 2600–2080 and 1100–1080 cal BP. These units are characterized by the lowest  $a^*$  and low  $b^*$  proxy values, indicating the blue-greyish colouration of the sediment. The amount of terrigenous material is high, while Ca, Sr, and TIC have minima here. TOC/TN values are slightly elevated. The grain size is slightly coarser here, notably in unit 9, as indicated by the GSD. The  $\log(\text{Rb}/\text{Sr})$  proxy is high in these units (Fig. 4).

Cluster 2 encompasses the thin, reddish units 11 (1830–1820 cal BP), 12 (1820–1770 cal BP), and 14 (1500–1420 cal BP), as well as units 9 (2600–2420 cal BP) and 18 (110–90 cal BP). While the three of reddish colour have high  $a^*$  values and low  $b^*$ , the latter are of blue-greyish colouration with low  $a^*$  and  $b^*$  proxy values (Fig. 3). The geochemical values are similar for all units with very high terrigenous input and local minima in carbonate input (Ca, Sr, and TIC). Unit 11 contains a considerably higher amount of quartz.  $\log(\text{Rb}/\text{Sr})$  shows maxima in all these units.

Cluster 3 is the largest cluster comprising all units belonging to the homogeneous greyish marls (units 10b, 10d, 13, 15, 17a, 17b). The  $a^*$  and  $b^*$  values indicate average values with an increasing trend with time towards more yellowish

**Table 2.** Sedimentary units of TRI1 with detailed sedimentological description. The sediment type classification follows the German ad-hoc Arbeitsgruppe Boden (2005; UB: upper boundary, G: gradational, P: planar).

Core depth (cm)	Sediment unit	Unit thickness (cm)	Munsell colour	Soil type	Description
0–32	19	32	2.5Y 4/3 olive brown	Ut4	more yellowish than 17b – terrigenous input (UB = sediment–water interface)
32–37	18	5	Gley 1 4/5 GY olive grey	Ut3	silty blue-greyish unit, similar to unit 16 (UB = G)
37–166	17b	129	5Y 6/3 olive grey	Ut3	matrix becomes darker and more yellowish, brown mottles, 0.85–1.0 m thin horizontal grey-blueish lines visible, 0.945 thin reddish line, more oxidation (UB = P)
166–189	17a	23	5Y 5/2 olive grey	Ut3	homogeneous grey matrix (UB = G)
189–193	16	27	Gley 1 4/5 GY olive grey	Ut3	thin blue-greyish layer (UB = P)
193–243	15	50	5Y 5/2 olive grey	Ut3-Ut4	homogeneous grey matrix, orange mottled (UB = P)
243–256	14	13	2.5YR 5/1 reddish grey	Ut3	similar to unit 12, gradual brightening towards top (UB = G)
256–295	13	39	5Y 5/2 olive grey	Ut3	homogeneous grey matrix, occasional black particles (UB = P)
295–303	12	8	2.5YR 4/1–4/2 dark reddish grey– weak red	Ut3	clayey silt, upper boundary with bubbly intrusions, gradual brightening towards top (UB = G)
303–305	11	2	2.5 YR 4/4 reddish brown	Ut4	compact, homogeneous, clearly defined boundaries (UB = P)
305–315	10d	10	5Y 5/2 – 6/2 (light) olive grey	Ut4	similar to 10b, homogeneous grey matrix (UB = strongly P)
315–317	10c	2	2.5Y 4/1 dark grey	Ut3	tephra layer, more strongly present in TRI1-B, coarser silt, larger pores (UB = P)
317–347	10b	30	5Y 5/2 – 6/2 (light) olive grey	Ut4	homogeneous grey matrix, more compact than 10a, charcoal particles (UB = G)
347–405	10a	58	5Y 5/2 olive grey	Ut3	grey matrix, black streaks, orange mottled, number of degassing holes decreases, gradually more compact (UB = G)
405–437	9	32	5Y 4/1 dark grey	Ut2	no macrofossils in whole core, extremely silty, small holes may indicate degassing (UB = G)

colouration. The highest amount of carbonates and the lowest log(Rb/Sr) values are found in this cluster.

Cluster 4 represents only the uppermost sedimentary unit 19, which covers the period 90–68 cal BP (1860–2018 CE). It is characterized by increasing terrigenous elements and decreasing carbonate content, which are more strongly increasing since 1970 CE (uppermost 10 cm). In this phase, the highest values for  $a^*$  and  $b^*$  colour proxies are reached, indicating the most intensive orange colouration. The Mn profile

is very noisy here, generally indicating higher values than before. The exclusion of this unit as a single cluster suggests that the environmental conditions for this period are significantly different from the preceding times.

The clusters show a large coherence with the visually observed differences in the sedimentary units. The clusters 1 and 2 contain all units with reddish and blueish colouration, while clusters 3 and 4 comprise the greyish marls. Due to the blueish colouration, units 9 and 18 were rather expected to

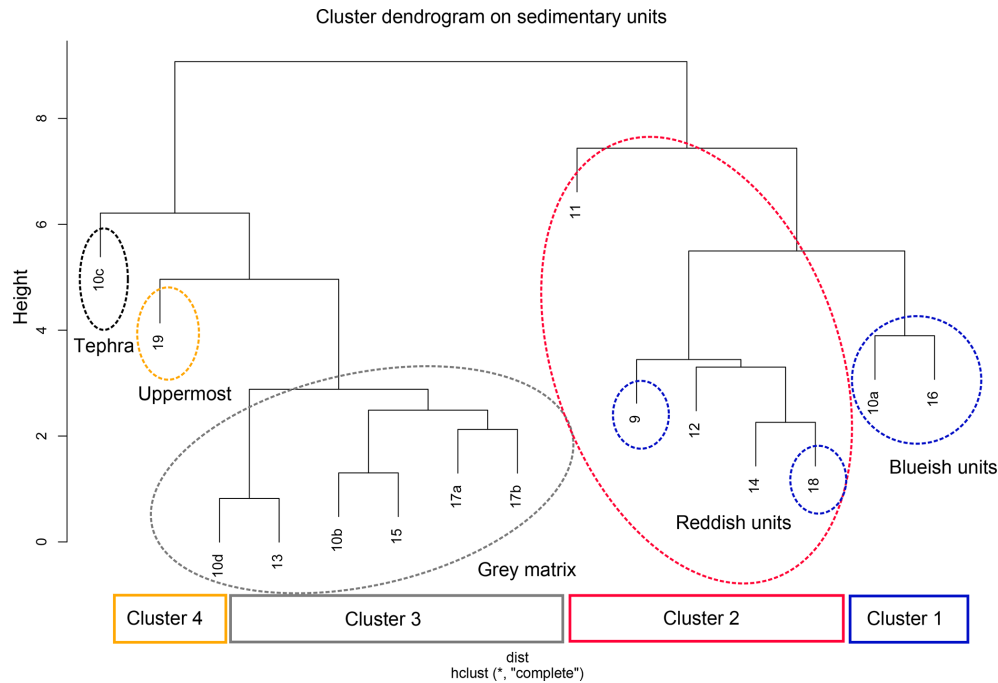


**Figure 6.** Dendrogram obtained by the hierarchical cluster analysis. The XRF elements and  $L^*a^*b^*$  colour values were used as input variables.

group into cluster 1. It is important to keep in mind that the results strongly depend on the chosen set of input variables (Khamnueva-Wendt et al., 2019). Slight differences in the clusters were observed when a different set of variables was selected, and diverse options including different sets of input variables, e.g. including the results of the principal component analysis (PCA), have been calculated. It became obvious that the larger dichotomous pattern, dividing the core into the more calcite-rich matrix on the one hand and the reddish and blueish coloured layers on the other, remained unchanged, even if a few sedimentary units were sub-clustered differently.

#### 4.3.2 PCA

A principal component analysis was conducted on 11 geochemical elements (Al, Si, K, Ca, Ti, Mn, Fe, Co, Rb, Sr, Zr) to reduce the multivariable dataset to a limited amount of uncorrelated components. The first three principal components (PC) cover > 80 % of the data information and were thus further analysed in more detail. Figure 7a shows the correlations between the element loadings and the PCs. Elements which show the same variation and whose loadings cluster together are likely influenced by the same environmental processes. The first principal component captures 44.8 % of the variance and spans the axis between carbonate-rich (Ca, Sr) on the negative axis and mainly mineral-rich assemblages (Zr, Rb, Fe, Ti; Fig. 7b) on the positive axis. A similar distribution has been found in other studies from the area (Em-

manouilidis et al., 2019; Katrantsiotis et al., 2018; Seguin et al., 2019, 2000).

The point cloud reveals that the lowermost part of the core (units 9, 10a; ca. 2600–2100 cal BP) plots on the positive side of the axis and is strongly dominated by clastic material (Fig. 7c). It corresponds mainly to cluster 1 and 2. The middle part of the core (ca. 2100–100 cal BP) alternates between positive and negative values with a focus in the upper left quadrant, with it being more strongly influenced by carbonate precipitation. It consists notably of cluster 3. The uppermost approximately 50 cm (the last ca. 150 years) shifts towards more positive PC1 scores again, showing an increase in detrital input. This part is classified as cluster 4. Similar fluctuations can be observed in the  $\log(\text{Rb}/\text{Sr})$  proxy plotted over time (Fig. 7d), or alternatively  $\log(\text{Ca}/\text{Ti})$  can be used (Seguin et al., 2020a). The Spearman correlation between  $\log(\text{Rb}/\text{Sr})$  and PC1 shows an extremely high conformity ( $r_{\text{Spearman}} = 0.95$ ), and thus here these two proxies are assumed to reflect the most important sedimentation changes in the lake catchment.

PC2 is positively associated with Al, Si, and K, while the loadings of the other elements are of minor importance (Fig. 7a). It has a high variance and the interpretation is not straightforward; it could potentially be linked to changes in material provenance.

PC3 is clearly dominated by Mn and has only a minor contribution of the loading of all the other elements (Fig. 7a). A correlation between PC3 and Mn/Fe ( $r_{\text{Spearman}} = 0.72$ )

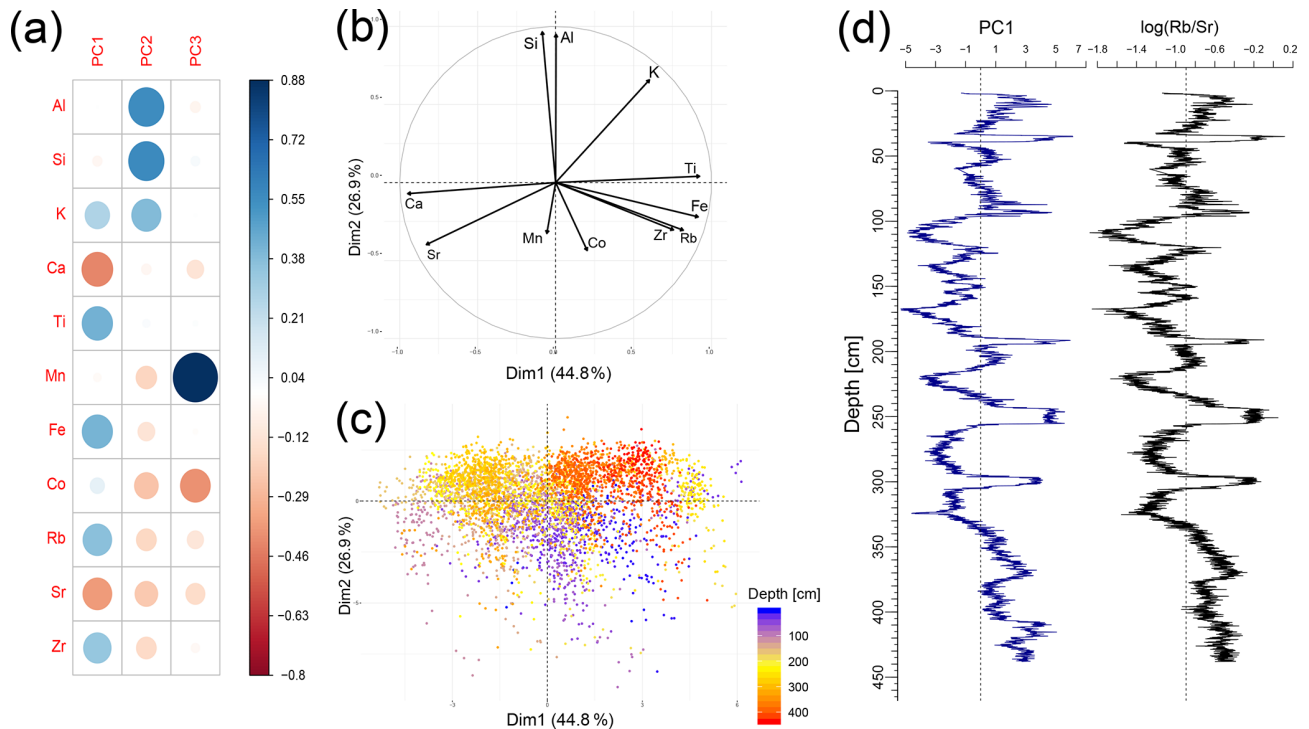


**Figure 7.** Principal component analysis (PCA) based on the centred log-ratio-transformed XRF data. **(a)** Correlation matrix between original elements and principal components (PC) 1–3. **(b)** Variable correlation circle displaying the correlation between PC1 and PC2. **(c)** Distribution of the sample points in the PC1–PC2 scatterplot. The samples are coloured according to their depth in the sediment core from purple (surface) to red (maximum depth). **(d)** PC1 and  $\log(\text{Rb}/\text{Sr})$  are plotted against depth and show a high conformity.

yields high conformity and suggests that PC3 may hint towards changes in the redox conditions at the lake bottom.

## 5 Discussion

### 5.1 Chronology

To support our radiocarbon chronology, we were looking for independent age indicators. One was found in TRII in the form of a tephra layer at 315–317 cm, lithologically classified as unit 10c (Fig. 3). In the XRF data, Rb, K, Zr and Sr values have a high peak here. Usually, Sr substitutes for Ca mainly in carbonate or sulfate minerals and co-precipitate in lakes, but it also occurs in magmatic rocks as part of Ca-rich plagioclase feldspars (Cohen, 2003; Kylander et al., 2011). This is the only unit in which Rb and Sr correlate, instead of anti-correlating, which suggests that the Sr supply here originates from an allochthonous, minerogenic source, e.g. plagioclase feldspars (Dypvik and Harris, 2001; Kylander et al., 2011). This layer was already found around 310 cm by Bottema (1980) and Creer et al. (1981) and described as a tephra layer. Based on geomagnetic and palynological investigations, Creer et al. (1981) concluded that due to the wind direction this tephra could be associated with the Somma-Vesuvius eruption in 79 CE that buried the city of Pompeii. Bottema (1982, 1980) argued based on palynological investi-

gations that the tephra should more likely be associated with the Santorini eruption, which can be rejected based on the recent reconstructions of the pathway of the ash plume (Johnston et al., 2012). In our age model, this layer dates to 1985–1789 cal BP at 316 cm and would thus be in accordance with the Pompeii eruption in 79 CE (1875 cal BP).

In a recent publication, Insinga et al. (2019) mapped tephra for the period 2000 to 4200 cal BP in the central Mediterranean. Stratigraphically right below the 79 CE eruption, they report a new horizon, the “FG/Lipari undefined layer”, originating from an unknown eruption dated to the time interval  $2187 \pm 37$  to 1970 cal BP. This eruption, which was found at different sites throughout the Ionian Sea (Insinga et al., 2019), also overlaps with the age uncertainty range of our tephra layer and could have also caused the tephra. The Pompeii eruption as well as the newly reported Lipari eruption would both support our age-depth model.

Another independent age marker was found by Bottema (1982) in the form of the presence of maize (*Zea mays*) at 110 cm, which according to Bottema needs to be younger than 250 years but unequivocally after 1492 CE (458 BP), the date of discovery of the New World. The main spread of maize in the Mediterranean was observed for the 16th and 17th century CE (Bintliff, 2012). Our model dates to 554 cal BP (419–701 cal BP) at 110 cm in TRII, and, assum-

ing that the depths were comparable in the cores from both studies, it would be slightly too old in the uppermost part.

During the first lake studies, radiocarbon dating on the sediments was challenging and methodological approaches were less advanced. Due to the high sedimentation rate of approximately  $1.7 \text{ mm yr}^{-1}$ , the core sequence in principle provides palaeoenvironmental information in annual resolution. However, even though our age-depth model is based on terrestrial macro-remains, it only provides an average probability range of 278 years. Hence, we do not discuss our data on an annual but rather on a multi-decadal to centennial scale. Nevertheless, within the constraints of the age-depth model, we can be more precise about the duration of periods and events than about absolute timing. The presented TRI1 core sequence continuously covers the last 2600 cal BP over more than 4 m of sediments, which is – though not laminated – a much higher temporal resolution than any other geoarchive from the area provided so far.

### 5.2 Event layers

Five lithological units of only few centimetres thickness depict a very different colour compared to the remaining sequence (units 11, 12, 14, 16, and 18, Fig. 3). Their lower sediment boundaries can always be classified as being flat and sharp but not erosive. If these units were the result of an immediate mass movement or turbidite event, one would expect an abrupt increase in coarser material and a sorting with a fining upwards gradient within these units (Sabatier et al., 2017; Wilhelm et al., 2016), which is not possible to identify from the presented analyses. Mn rises steeply at the onset of the units, followed by a gradual decrease within the respective units (Fig. 4). This pattern suggests bottom water oxygenation (Calvert and Pedersen, 1993) triggered by an abrupt (ventilation) event, as during turbidite formation, which caused Mn enrichment and the changes in colour. Afterwards, the system gradually re-gained its initial status. This would support the hypothesis that the reddish and blueish units were deposited during or following short-term events. We also elaborated on the option that the units could have been deposited at once, e.g. by a turbidity current, treating these units as mass movement events during the age modelling process. The respective age model overlapped completely within the uncertainty range of the model without specific event layers (see Fig. S3). Hence, we decided to use the model with continuous sedimentation as the final age-depth model.

As the region is characterized by high seismo-tectonic activity (Taymaz et al., 2007), one plausible trigger causing turbidity currents or mass movement events could have been earthquakes. A connection between earthquakes and terrestrial landslides and rock falls has been investigated for the region by Papadopoulos and Plessa (2000). Due to the frequent occurrences of earthquakes, however, it seems impossible, respecting the age uncertainty range, to assign the red-

dish and blueish units to specific earthquakes from the catalogue (Papadopoulos et al., 2014).

### 5.3 Sedimentary facies interpretation

The cluster analysis emphasizes similarities between certain sedimentary units of TRI1 based on their colour and geochemical characteristics. As these sediment characteristics are affected by the palaeoenvironmental conditions during deposition, the dendrogram classification may be used to infer phases with similar palaeoenvironmental conditions. Four different facies were identified during the cluster analysis (Fig. 6).

Cluster 1 is interpreted as compiling phases with higher terrigenous input and bottom water oxygenation, which was caused by rather abrupt changes in the environmental conditions, e.g. by intensive precipitation. The higher terrigenous input is interpreted as an indicator of catchment erosion during wetter conditions. The values of PC1 are high during these phases.

Cluster 2 shows likewise a higher amount of detrital material that was transported into the lake. The different colouration of the sediments in both clusters suggests different processes to have influenced their deposition, but it is not possible to unequivocally identify the sedimentary process, as different influential factors would lead to increasing clastic input. Wetter conditions with more intense winter precipitation may have been one trigger. Another possible trigger could have been summer storm events that would break down or disturb the stratification in the water column and increase run-off intensity, which would most likely also result in turbulent and coarser sediment deposition. Furthermore, one may also expect an increasing amount of micro- and macrofossils, e.g. broken shells or higher organic matter content, which was washed in and deposited before decomposition, which we do not observe here. Human impact, e.g. by deforestation, is also known to increase erosion and detrital material input (Meriam et al., 2018). However, one would expect longer-lasting periods, while these facies units lasted a maximum of 100 years. We interpret cluster 2 also as indicating wetter conditions and attribute the variation in colour compared to cluster 1 to differences in the Mn and Fe oxides (Statham et al., 2017). PC1 likewise shows highest values in this cluster.

The majority of the core is composed of the greyish marls in cluster 3, which have a homogeneous appearance, although the geochemical ratios show intense fluctuations within these units, most likely reflecting a higher variability in palaeoclimate. It is assumed that sediments in this cluster were deposited within a stable, stratified lake ecosystem with anoxic bottom water conditions. Variations in the XRF data may be explained by palaeoclimatic variation. The high Ca content may be linked to intense carbonate precipitation under warm and dry conditions. The PC1 values are mostly negative in this cluster.

The uppermost sedimentary unit forms cluster 4 by itself and is interpreted as potentially being influenced by anthropogenic activity in the catchment. It seems as if human activity in the area has been increasing since the 1860s and has intensified particularly since 1970 CE with the sudden increase in  $a^*$  or that its impacts have increasingly reached the coring spot, e.g. through run-off from cultivated, fertilized fields. Mn values in this unit are higher than in unit 3 and have a high variance, potentially indicating instability in the modern monomictic conditions that supply oxygen to the hypolimnion. The PC1 values in this unit gradually shift from negative to positive and back, and it is likely that the climatic signal here was disturbed by human influence.

## 5.4 Palaeoenvironmental reconstruction for the last 2600 years in comparison to other regional archives

### 5.4.1 Human history in Aetolia

Lake Trichonida has been studied irregularly since the 1980s (for example Albrecht et al., 2009; Bottema, 1982, 1980; Dimitriou and Zacharias, 2006; Koussouris and Diapoulis, 1982; Tafas et al., 1997). Archaeological research in Aetolia is comparatively weak, as the area was and still is rather thinly populated, but it confirms human activity since the Late Helladic period (1700–1100 BCE/3650–3050 BP; Bommeljé and Doom, 1987; Haenssler et al., 2013). Bommeljé and Doom (1987) consider a population peak in the region during the Classical–Hellenistic period (479–31 BCE/2429–1981 BP) and only few traces of human presence throughout Roman and Byzantine times (31–1460 BCE/1981–490 BP). The closest major archaeological site is Thermos, which was occupied since the Bronze Age, had its flourishing stage during the Middle Helladic period (2100–1700 BCE/4050–3650 BP), and was the centre of the Aetolian League (Papapostolou, 2012). In a recent comparative study on land use and demography in Greece by Weiberg et al. (2019), Thermos was the only site in Aetolia-Acarnania that was included, underlining the scarcity of data in this region. A similar picture can be found in the meta-analysis on demography, climate, and erosion by Walsh et al. (2019), which includes six Greek sites but completely leaves out western Greece. They state high levels of human activity during the Classical and Roman period for southern Greece, which is in contrast with the assumptions by Bommeljé and Doom (1987). These findings stress that deduced demographic trends from both analyses cannot necessarily be transferred to the remote area around Lake Trichonida.

The closest palaeoenvironmental archive for comparison is Etoliko (also known as Aitoliko) Lagoon (Koutsodendris et al., 2015, 2017; Haenssler et al., 2013). The sedimentation rate at Etoliko Lagoon since 1350 cal BP was calculated at  $2.1 \text{ mm yr}^{-1}$  and is thus in a similar range like at Lake Trichonida. Before, it was calculated at  $0.4 \text{ mm yr}^{-1}$ , and Haenssler et al. (2013) interpret the drastic change as a causal relationship with increasing anthropogenic land use and set-

tlement activity. In Trichonida, we do not have comparative numbers from earlier times. As we do not have indications for sudden changes, we suppose that small numbers of humans were always present in the study area during the last 2600 years but had a rather marginal influence on the lake development. They were probably not responsible for the creation of the blueish-reddish layers of cluster 1 and 2. However, due to land use activities, they may have indirectly provided loose material that could have been eroded more easily during strong precipitation events.

In an earlier pollen study, Bottema (1982) identified 71 pollen types from the “plant-sociological relevé list” at Lake Trichonida. The AP/NAP ratio of arboreal vs. non-arboreal pollen types was reproduced and is shown in Fig. 8k. As Bottema (1982) abstained from creating an age-depth model, we used our model to plot the data on a timescale, assuming that the depth scales of the two cores were comparable, which is also suggested by the sediment depth of the tephra unit differing by only 5 cm. Overall, the number of pollen types correlated positively with the AP/NAP ratio (Bottema, 1982), which means that land opening increased the pollen diversity and lower AP/NAP values hint towards natural or anthropogenic deforestation. Dense *Abies cephalonica* woodland could be found in the mountainous regions in southern Greece until human deforestation (Jahns, 1993). The lowest degrees of forestation are depicted in Bottema’s (1982) pollen diagram for the period 2600–2000 cal BP, which is considered as a period with a population peak (Bommeljé and Doom, 1987; cluster 1). The continuous presence of *Vitis* pollen confirms our hypothesis of rather constant, but low human influence in the area for the investigated period. The highest arboreal pollen amounts can be observed during the wet phases of the reddish units in cluster 2. Apart from that, the resolution is too coarse to reasonably compare it to the XRF proxies.

### 5.4.2 Palaeohydrological changes

For the last 2600 years, Lake Trichonida shows different phases of palaeohydrological fluctuation. It has witnessed several phases of wetter or drier climatic conditions, as observed in the  $\log(\text{Rb}/\text{Sr})$  and PC1 proxies.

Rb can replace K in the crystal lattice in feldspars and it is associated with clay mineral assemblages (Heymann et al., 2013; Koinig et al., 2003). As Rb, associated with terrigenous sediment input, and Sr, associated mainly with carbonates, show a very different geochemical behaviour, the Rb/Sr ratio is often interpreted as a proxy for chemical weathering (Jin et al., 2006; Xu et al., 2010). While carbonates can be associated either with carbonate weathering in the catchment or with authigenic precipitation of chemical or biogenic carbonates in the lake, notably during dry and warm phases, the clastic elements originate from terrestrial input eroded during wet periods with enhanced precipitation and run-off (Cohen, 2003; Kylander et al., 2011). High Sr values are interpreted

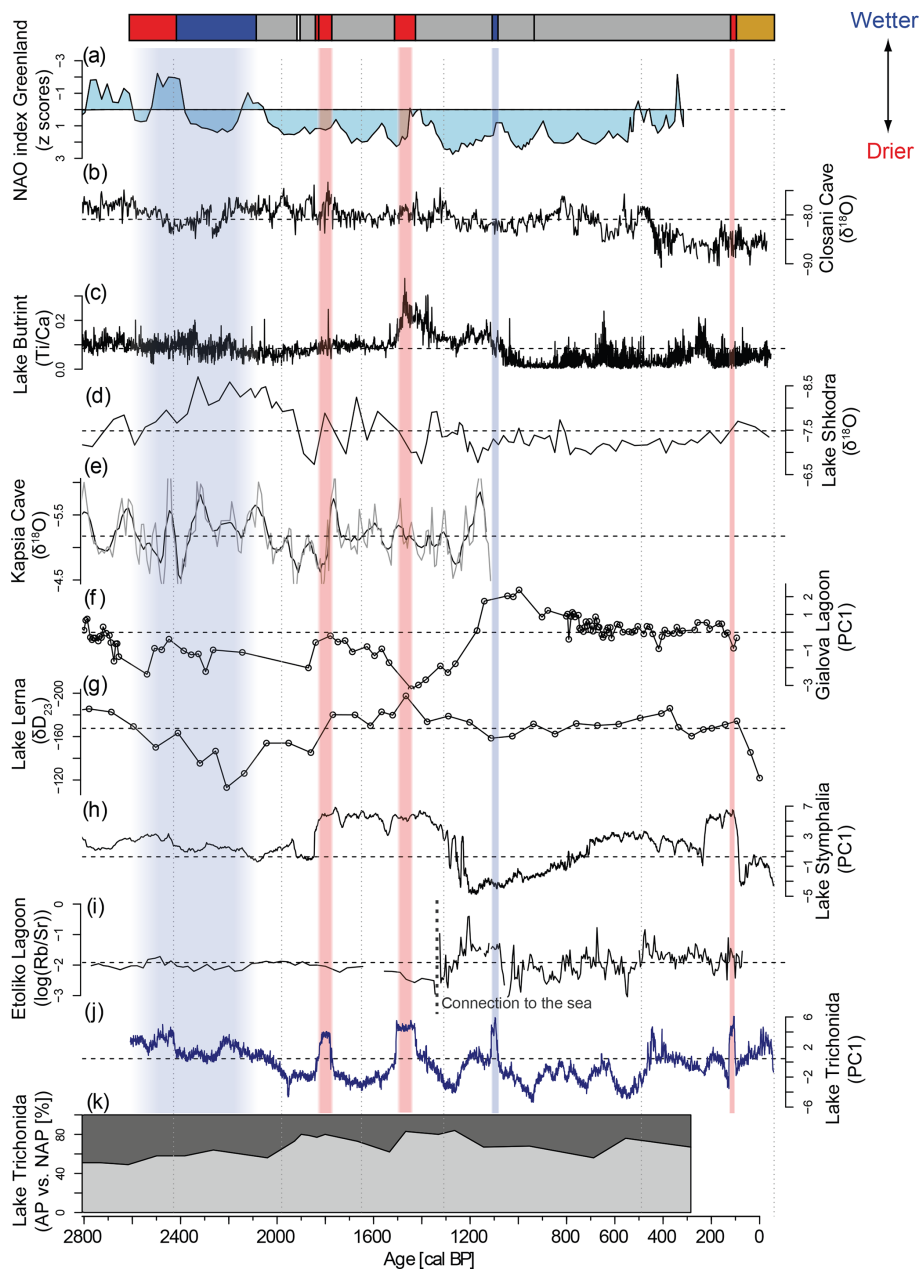


**Figure 8.** Comparison of the PC1 proxy with other regional hydroclimate records. (a) NAO index reconstruction from a lake in SW Greenland (axis inverted) from Olsen et al. (2012). (b) Autumn/winter precipitation reconstruction from a speleothem at Closani Cave (SW Romania; Warken et al., 2018). (c) Ti/Ca proxy from Lake Butrint (Albania; Morellón et al., 2016). (d)  $\delta^{18}\text{O}$  record from Lake Shkodra (axis inverted; Zanchetta et al., 2012). (e)  $\delta^{18}\text{O}$  record from a speleothem in Kapsia Cave (axis inverted; Finné et al., 2014). (f) PC1 on XRF data from Gialova Lagoon (Katrantsiotis et al., 2018). (g)  $\delta\text{D}_{23}$  proxy from Lake Lerna (axis inverted; Katrantsiotis et al., 2019). (h) PC1 on XRF data from Lake Stymphalia (Seguin et al., 2019). (i)  $\log(\text{Rb}/\text{Sr})$  ratio from Etoliko Lagoon (Haenssler et al., 2013). (j) PC1 on XRF data from Lake Trichonida (this study). (k) Arboreal (AP) vs. non-arboreal pollen (NAP) from Lake Trichonida (data reconstructed from Bottema (1982) plotted against our chronology). Values plotted to the top generally indicate wetter conditions. Vertical shaded bars indicate relatively more humid phases at Lake Trichonida (see text for more detail). Vertical dashed lines indicate cultural unit boundaries according to Weiberg et al. (2016). The results of the cluster analysis are plotted at the top.

to generally indicate higher carbonate precipitation under warm and/or more arid conditions, while higher Rb values hint towards stronger physical weathering of clastic material and enhanced surface run-off related to increased precipitation during colder and wetter conditions (Unkel et al., 2014). As PC1 reflects the same variation between carbonate-rich and mineral-rich assemblages, it is interpreted similarly (see Sect. 4.3.1). A similar distribution has been found in other studies from the area and was interpreted as reflecting hydro-climatic variations (Emmanouilidis et al., 2019; Katrantsiotis et al., 2018; Seguin et al., 2019).

We assume that the lake level has fluctuated over a few metres – modern inter-annual variation is about 1 m (Tafas et al., 1997) – but due to its depth and the sedimentary characteristics, we exclude the option of complete desiccation, as it was shown for shallow lakes in southern Greece (Seguin et al., 2020a).

From around 2600 to 2000 cal BP, PC1 generally shows a decreasing trend towards drier conditions in the study area with a minimum occurring around 2000–1800 cal BP. Olsen et al. (2012) reconstructed a high-resolution NAO index for the last 5200 years based on a *z* score on geochemical data from a lake sediment record from southwestern Greenland that reflects large-scale variability in the Northern Hemisphere climate. Their NAO index for the interval 2400–2000 cal BP also shows a predominantly increasing trend that is likewise connected with drier climatic conditions (Olsen et al., 2012, Fig. 8a). Centring around 2500 and 2200 cal BP, two short periods with slightly wetter conditions can be identified in the general trend of the PC1 record, when it becomes more positive, and are largely in agreement with the negative NAO indices. Katrantsiotis et al. (2019) suggest that the North Atlantic Oscillation controls the climate in Greece notably during winter. When the NAO index is positive, the westerlies are stronger than usual and the humid air masses run further north, leading to drier and colder winters in Greece, while negative NAO indices relate to wetter and warmer conditions (Katrantsiotis et al., 2019; Koutsodendris et al., 2015; Nieto-Moreno et al., 2011).

Drying climate conditions before 2000 cal BP are also reported from Lake Lerna, NE Peloponnese (Katrantsiotis et al., 2019, Fig. 8g); the Asea valley, central Peloponnese (Unkel et al., 2014); and Skala Marion Cave, 350 km to the NE on the Greek island of Thassos (Psomiadis et al., 2018). Unlike these archives, Lake Malik, 250 km to the north at the border with Albania (Fouache and Pavlopoulos, 2010), and Lake Shkodra, 450 km to the north at the border between Albania and Montenegro (Zanchetta et al., 2012, Fig. 8d), as well as the Agios Floros fen, S Peloponnese (Norström et al., 2018), reveal a trend towards wetter conditions during the same period from 2600 to 2000 cal BP. The resolution of the  $\delta D_{23}$  record from Agios Floros (Norström et al., 2018), however, is too low to reasonably compare the record to Lake Trichonida. This inconsistent observation is in general agreement with Finné et al. (2011), who summarize the hydrolog-

ical situation during this time period as an incoherent picture without “discernable spatial patterns”. They report generally warmer temperatures, which would be in agreement with the increase in carbonates in the sediment sequence at Trichonida.

This drier/warmer phase ends abruptly around 1750 cal BP with a rapid increase in terrigenous material input into Lake Trichonida, most likely due to increased precipitation and surface run-off in the catchment. Lithologically, this period corresponds to the very distinct reddish units 11 and 12 (Fig. 3). Closani Cave (Warcken et al., 2018, Fig. 8b), Kapsia Cave (Finné et al., 2014, Fig. 8e), Lake Lerna (Katrantsiotis et al., 2019, Fig. 8g), and Skala Marion Cave (Psomiadis et al., 2018) all provide evidence for higher humidity for the period around 1800 cal BP. Lake Shkodra (Fig. 8d) and Gialova Lagoon (Fig. 8f) also give evidence for a short wetter period, but from a medium term perspective the proxies rather follow a drying trend lasting until 1400 cal BP (Katrantsiotis et al., 2018; Zanchetta et al., 2012). Interestingly, this wet century at Lake Trichonida coincides with the aqueduct construction at Lake Stymphalia, which was interpreted as triggering the abrupt shift in the PC1 proxy (Seguin et al., 2019, Fig. 8h). The AP/NAP ratio depicts an increase in arboreal pollen for 2050–1800 cal BP (Bottema, 1982, Fig. 8k), which on the one hand supports the wetter conditions favourable for tree growth. On the other hand, an increasing input of terrigenous material, e.g. also caused by increasing land use, may generally induce a larger quantity of pollen from the catchment in the sample, and a transformation in the pollen transport process may influence the spectrum composition in the sample. A similar coincidence occurs in 1500 cal BP; an abrupt increase in terrigenous material coincides with an increase in the AP/NAP ratio.

The interval, ca. 1700–1500 cal BP (250–450 CE), can be interpreted as a phase of stable, drier conditions at Lake Trichonida. Kapsia Cave (Finné et al., 2014) and Closani Cave (Warcken et al., 2018) also show relatively stable conditions, and the NAO index is solely positive although variable (Olsen et al., 2012, Fig. 8a). For Anatolia and the Levant, Izdebski et al. (2016) speak of a late Roman drought lasting from ca. 1600 to 1480 cal BP (350 to 470 CE), which was then followed by a dramatic shift to much wetter climatic conditions.

An abrupt shift to wetter conditions can also be observed at Lake Trichonida in ca. 1500 cal BP that lasts about 100 years. It almost coincides with an abrupt shift towards a slightly negative, neutral NAO index and the wettest period at Lake Lerna (Katrantsiotis et al., 2019). The highest values of the Ti/Ca proxy, indicating increasing run-off under wetter conditions, at Lake Butrint also fall exactly in this phase (Morel-lón et al., 2016). Wetter conditions are reported from various sites in the eastern Mediterranean region for approximately 1600–1200 cal BP (350–750 CE; Finné et al., 2011; Haliuc et al., 2017; Seguin et al., 2019). In central and northern Europe this period is known as the Late Antique Little Ice Age or

Migration Period and experienced colder and more arid climatic conditions (Büntgen et al., 2016; Helama et al., 2017; McCormick et al., 2012).

During the following millennium, PC1 at Lake Trichonida alternates between drier phases (1350–1200, 1050–900, 800–650, and 600–450 cal BP), intermediate phases, and shorter wet spells (around 1100, 450–300, and around 120 cal BP). With a slight offset, most likely due to dating uncertainties, the wet spells broadly correlate with more negative NAO indices. Probably due to its coarse resolution, the AP/NAP ratio is unaffected by these fluctuations and shows a constant decrease between 1250 and 700 cal BP (700–1250 CE) which may hint towards human deforestation activity. The period lasting approximately from 1000 to 700 cal BP (950–1250 CE) is often referred to as the Medieval Climate Anomaly and is generally considered a period with warmer temperatures on the Northern Hemisphere (Luterbacher et al., 2012; Mann et al., 2009; Roberts et al., 2012). According to Finné et al. (2011), its beginning can be characterized by generally wetter conditions in the eastern Mediterranean. The Lake Trichonida proxy indicates drier or warmer conditions for the period 1050–900 cal BP.

At Lake Trichonida, PC1 shows strong oscillations of century-long wetter and drier periods, which generally suggest more unstable hydroclimatic conditions. Around 650–600 and 450–ca. 350 cal BP, we see decades with wetter conditions, while the period in between (ca. 600–500 cal BP) indicates a very dry period. The curve progression of the Etoliko Lagoon largely resembles this pattern (Fig. 8i). The period of the Little Ice Age, approximately 700–200 cal BP (1250–1750 CE), is generally characterized by colder conditions and glacier advances in the Alps (Magny et al., 2012; Mann et al., 2009) and by wetter conditions in the Mediterranean (Roberts et al., 2012) and on the Peloponnese (Katrantsiotis et al., 2019). The NAO index is more variable at this time, generally showing drier conditions in the first half of the period shifting to wetter conditions and more negative values around 550 cal BP (Olsen et al., 2012). Lake Butrint generally depicts increased clastic input during wetter conditions for the LIA (Morellón et al., 2016, Fig. 8c). Lake Lerna shows slightly wetter conditions for 700–350 cal BP, followed by a progressive drying (ca 250–100 cal BP; Katrantsiotis et al., 2019), and the Gialova  $\delta D_{31}$  profile also shows a period of wetter conditions (700–300 cal BP; Katrantsiotis et al., 2018). At these sites, the LIA looks like a period with very stable hydroclimatic condition, in contrast to Trichonida, which may however be attributed to the low resolution of the proxies. The youngest and shortest wet period (sedimentary unit 18) around 120–100 cal BP (1830–1850 CE) is not visible in any other archive. Based on the Etoliko record, Koutsodendris et al. (2017) suggested that the Mediterranean see-saw precipitation pattern oscillated longitudinally during the LIA, shifting the wet–dry boundary between the western and eastern Mediterranean, which could also explain the variable pattern observed at Lake Tri-

chonida. However, more high-resolution records or palaeoreconstructions of the different teleconnection patterns would be needed to support this assumption.

For the last ca. 150 years, notably the 20th century CE, we observe an increasing trend in PC1, except for the last ca. 20 years, that would indicate increasingly wetter conditions. More intense anthropogenic impact causing soil erosion, however, would cause a similar signal, and it thus seems possible that human activity blurs the climatic signal for this period (Seguin et al., 2019; Zanchetta et al., 2012). The different colour in sedimentary unit 19 (Fig. 3) and the singularity of cluster 4 (Fig. 6) would support this hypothesis. However, this is not in agreement with findings from Koutsodendris et al. (2015), who detect NAO-related precipitation patterns for the second half of the 20th century at Etoliko Lagoon, 20 km SE of Lake Trichonida, and a decrease in winter precipitation since the 1980s. Additionally, they noted strong land use changes only since the early 1980s onwards (Koutsodendris et al., 2015).

## 6 Conclusion

The multi-proxy data from Lake Trichonida shows palaeoenvironmental, notably palaeohydrological, changes for the last 2600 years for a region, where high-resolution climate records are sparse, but which would be essential to understand variation in the hydrological pattern in the past in this transitional zone between two different climatic zones. According to their sedimentology, four main facies clusters were identified and described by Lake Trichonida, supported by fast and cheap high-resolution imagery and the analysis of colour variations.

Evidence of anthropogenic impact on the landscape was only clearly observed for the last ca. 100 years. Before, climatic fluctuations may have been more decisive than human impact from the very sparsely settled landscape.

The majority of the observed fluctuations in Lake Trichonida were contemporaneous with phases of a more negative NAO index, as reconstructed by Olsen et al. (2012), and thus our record suggests a connectivity between local hydrological variation and the North Atlantic Oscillation on centennial timescales. Our study suggests that during the last 2600 years Lake Trichonida and the eastern Mediterranean/Carpathian region (namely Lake Butrint, Lake Shkodra) are linked by the same moisture source and a positive NAO index regionally translates to drier conditions in the study area. Due to the spatial heterogeneity of the area and the location at a transitional climatic zone, the record also exhibits some local peculiarities such as the blueish and reddish sedimentary units that were triggered by short-term events, which have not been recorded or described from other sites. It thus seems coherent that the signal cannot fully be traced back to climatic oscillations, but additional forcing mecha-

nisms influenced the system and further research is necessary to identify these factors.

**Data availability.** The primary datasets can be found on PANGAEA: <https://doi.org/10.1594/PANGAEA.921324> (Seguin, et al., 2020b).

**Supplement.** The supplement related to this article is available online at: <https://doi.org/10.5194/egqsj-69-139-2020-supplement>.

**Author contributions.** JS conducted the lab work and statistical analyses and wrote the manuscript with contributions of IU, AE, and PA. AE conducted the measurement and evaluation of the XRD data and with PA supported the fieldwork and sampling campaign. JS and IU interpreted the data. IU designed the project and headed the fieldwork. WD provided the coring equipment and directed the coring proceeding during fieldwork.

**Competing interests.** The authors declare that they have no conflict of interest.

**Acknowledgements.** In alphabetical order, we kindly thank our following colleagues and students for their invaluable support in the field: Mathias Bahns, Ioannis Prevedouros, Evaggelos Tsiotsis, and Jan Weber. Yasmin Dannath, Sophia Dazert, McKenzie Elliott, and Clemens von Scheffer are acknowledged for support and assistance during laboratory work. We also thank two anonymous reviewers, and the associate editor Elisabeth Dietze for their valuable comments that helped to improve the manuscript. The project was carried out with the relevant permits from the Greek authorities, the Institute of Geology and Mineral Exploration of Greece (IGME), and the Water Management Body of the Decentralized Prefecture of Peloponnese, Western Greece and the Ionian Islands.

**Financial support.** This research has been supported by the Collaborative Research Centre 1266 “Scales of Transformation – Human-environmental interaction in prehistoric and archaic societies” of the German Research foundation (DFG, project no. 2901391021).

**Review statement.** This paper was edited by Elisabeth Dietze and reviewed by two anonymous referees.

## References

ad-hoc Arbeitsgruppe Boden: *Bodenkundliche Kartieranleitung*, E. Schweizerbart'sche Verlagbuchhandlung, Hannover, Germany, 2005.

Albrecht, C., Hauffe, T., Schreiber, K., Trajanovski, S., and Wilke, T.: Mollusc Biodiversity and Endemism in the Pot-

tial Ancient Lake Trichonis, Greece, *Malacologia*, 51, 357–375, <https://doi.org/10.4002/040.051.0209>, 2009.

Avramidis, P., Samiotis, A., Kalimani, E., Papoulis, D., Lampropoulou, P., and Bekiari, V.: Sediment characteristics and water physicochemical parameters of the Lysimachia Lake, Western Greece, *Environ. Earth Sci.*, 70, 383–392, <https://doi.org/10.1007/s12665-012-2134-9>, 2013.

Barnston, A. G. and Livezey, R. E.: Classification, Seasonality and Persistence of Low-Frequency Atmospheric Circulation Patterns, *Mon. Weather Rev.*, 115, 1083–1126, [https://doi.org/10.1175/1520-0493\(1987\)115<1083:CSAPOL>2.0.CO;2](https://doi.org/10.1175/1520-0493(1987)115<1083:CSAPOL>2.0.CO;2), 1987.

Bintliff, J. L.: *The Complete Archaeology of Greece, from Hunter-Gatherers to the Twentieth Century AD*, Blackwell-Wiley, Oxford, New York, USA, 2012.

Blaauw, M. and Christeny, J. A.: Flexible paleoclimate age-depth models using an autoregressive gamma process, *Bayesian Anal.*, 6, 457–474, <https://doi.org/10.1214/11-BA618>, 2011.

Bommeljé, S. and Doom, P.K.: *Aetolia and the Aetolians: Towards the Interdisciplinary Study of a Greek Region*, *Studia Aetolica I*, Utrecht, the Netherlands, 1987.

Bottema, S.: On the history of the walnut (*Juglans Regia* L.) in southeastern Europe, *Acta Bot. Neerl.*, 29, 343–349, <https://doi.org/10.1111/j.1438-8677.1980.tb01240.x>, 1980.

Bottema, S.: Palynological Investigations in Greece with Special Reference to Pollen as an Indicator of Human Activity, *Palaeohistoria*, 24, 257–288, 1982.

Büntgen, U., Myglan, V. S., Ljungqvist, F. C., McCormick, M., Cosmo, N. Di, Sigl, M., Jungclaus, J., Wagner, S., Krusic, P. J., Esper, J., Kaplan, J. O., Vaan, M. A. C. De, Luterbacher, J., Wacker, L., Tegel, W., and Kirilyanov, A. V.: Cooling and societal change during the Late Antique Little Ice Age from 536 to around 660 AD, *Nat. Geosci.*, 9, 231–237, <https://doi.org/10.1038/NGEO2652>, 2016.

Calvert, S. E. and Pedersen, T. F.: Geochemistry of Recent oxic and anoxic marine sediments: Implications for the geological record, *Mar. Geol.*, 113, 67–88, [https://doi.org/10.1016/0025-3227\(93\)90150-T](https://doi.org/10.1016/0025-3227(93)90150-T), 1993.

Christiansen, B. and Ljungqvist, F. C.: Challenges and perspectives for large-scale temperature reconstructions of the past two millennia, *Rev. Geophys.*, 55, 40–96, <https://doi.org/10.1002/2016RG000521>, 2017.

Cohen, A. S.: *Paleolimnology: the history and evolution of lake systems*, 1st edn., Oxford University Press, Oxford, UK, 2003.

Creer, K. M., Readman, P. W., and Papamarinopoulos, S.: Geomagnetic secular variations in Greece through the last 6000 years obtained from lake sediment studies, *Geophys. J. R. Astr. Soc.*, 66, 193–219, 1981.

Dimitriou, E. and Zacharias, I.: Quantifying the rainfall-water level fluctuation process in a geologically complex Lake catchment, *Environ. Monit. Assess.*, 119, 491–506, <https://doi.org/10.1007/s10661-005-9039-y>, 2006.

Dypvik, H. and Harris, N. B.: Geochemical facies analysis of fine-grained siliciclastics using Th/U, Zr/Rb and (Zr + Rb)/Sr ratios, *Chem. Geol.*, 181, 131–146, [https://doi.org/10.1016/S0009-2541\(01\)00278-9](https://doi.org/10.1016/S0009-2541(01)00278-9), 2001.

Emmanouilidis, A., Katrantsiotis, C., Norström, E., Risberg, J., Kylander, M., Sheik, T. A., Iliopoulos, G., and Avramidis, P.: Middle to late Holocene palaeoenvironmental study of Gialova

- Lagoon, SW Peloponnese, Greece, *Quatern. Int.*, 476, 46–62, <https://doi.org/10.1016/j.quaint.2018.03.005>, 2018.
- Emmanouilidis, A., Unkel, I., Triantaphyllou, M., and Avramidis, P.: Late-Holocene coastal depositional environments and climate changes in the Gulf of Corinth, Greece, *Holocene*, 30, 77–89, <https://doi.org/10.1177/0959683619875793>, 2019.
- European Environment Agency: NATURA 2000 – Standard Data Form: Limnes Trichonida kai Lysimacheia, Copenhagen, Denmark, available at: <https://natura2000.eea.europa.eu/Natura2000/SDF.aspx?site=GR2310009&release=10#7>, last access: 8 June 2020.
- Finné, M., Holmgren, K., Sundqvist, H. S., Weiberg, E., and Lindblom, M.: Climate in the eastern Mediterranean, and adjacent regions, during the past 6000 years – A review, *J. Archaeol. Sci.*, 38, 3153–3173, <https://doi.org/10.1016/j.jas.2011.05.007>, 2011.
- Finné, M., Bar-Matthews, M., Holmgren, K., Sundqvist, H. S., Liakopoulos, I., and Zhang, Q.: Speleothem evidence for late Holocene climate variability and floods in Southern Greece, *Quaternary Res.*, 81, 213–227, <https://doi.org/10.1016/j.yqres.2013.12.009>, 2014.
- Finné, M., Woodbridge, J., Labuhn, I., and Roberts, C. N.: Holocene hydro-climatic variability in the Mediterranean: A synthetic multi-proxy reconstruction, *Holocene*, 29, 847–863, <https://doi.org/10.1177/0959683619826634>, 2019.
- Fouache, E. and Pavlopoulos, K.: The Interplay between Environment and People from Neolithic to Classical Times in Greece and Albania, in: *Landscapes and Societies: Selected Cases*, edited by: Martini, I. P. and Chesworth, W., Springer, Dordrecht, Heidelberg, London, New York, 155–166, <https://doi.org/10.1007/978-90-481-9413-1>, 2010.
- Grootes, P. M., Nadeau, M.-J., and Rieck, A.: 14C-AMS at the Leibniz-Labor: radiometric dating and isotope research, *Nucl. Instrum. Meth. B*, 223–224, 55–61, <https://doi.org/10.1016/j.nimb.2004.04.015>, 2004.
- Haessler, E., Nadeau, M. J., Vött, A., and Unkel, I.: Natural and human induced environmental changes preserved in a Holocene sediment sequence from the Etoliko Lagoon, Greece: New evidence from geochemical proxies, *Quatern. Int.*, 308–309, 89–104, <https://doi.org/10.1016/j.quaint.2012.06.031>, 2013.
- Haliuc, A., Veres, D., Brauer, A., Hubay, K., Hutchinson, S., Begy, R., and Brauer, M.: Palaeohydrological changes during the mid and late Holocene in the Carpathian area, central-eastern Europe, *Global Planet. Change*, 152, 99–114, <https://doi.org/10.1016/j.gloplacha.2017.02.010>, 2017.
- Helama, S., Jones, P. D., and Briffa, K. R.: Dark Ages Cold Period: A literature review and directions for future research, *Holocene*, 16, 095968361769389, <https://doi.org/10.1177/0959683617693898>, 2017.
- Heymann, C., Nelle, O., Dörfler, W., Zagana, H., Nowaczyk, N., Xue, J., and Unkel, I.: Late Glacial to mid-Holocene palaeoclimate development of southern Greece inferred from the sediment sequence of Lake Stymphalia (NE-Peloponnese), *Quatern. Int.*, 302, 42–60, <https://doi.org/10.1016/j.quaint.2013.02.014>, 2013.
- Insinga, D. D., Petrosino, P., Alberico, I., Lange, G. J., Lubritto, C., Molisso, F., Sacchi, M., Sulpizio, R., Wu, J., and Lirer, F.: The Late Holocene tephra record of the central Mediterranean Sea: Mapping occurrences and new potential isochrons for the 4.4–2.0 ka time interval, *J. Quaternary Sci.*, 35, 213–231, <https://doi.org/10.1002/jqs.3154>, 2019.
- Institute of Geology and Mineral Exploration of Greece (IGME): Geological Map of Greece, 1 : 50 000 (Sheet Thermon), Athens, Greece, 1977.
- Institute of Geology and Mineral Exploration of Greece (IGME): Geological Map of Greece, 1 : 50 000 (Sheet Messolonghion), Athens, Greece, 1988.
- Izdebski, A., Pickett, J., Roberts, N., and Waliszewski, T.: The environmental, archaeological and historical evidence for regional climatic changes and their societal impacts in the Eastern Mediterranean in Late Antiquity, *Quaternary Sci. Rev.*, 136, 189–208, <https://doi.org/10.1016/j.quascirev.2015.07.022>, 2016.
- Jahns, S.: On the Holocene vegetation history of the Argive Plain (Peloponnese, southern Greece), *Veg. Hist. Archaeobot.*, 2, 187–203, <https://doi.org/10.1007/BF00198161>, 1993.
- Jin, Z., Cao, J., Wu, J., and Wang, S.: A Rb/Sr record of catchment weathering response to Holocene climate change in Inner Mongolia, *Earth Surf. Proc. Land.*, 31, 285–291, <https://doi.org/10.1002/esp.1243>, 2006.
- Johnston, E. N., Phillips, J. C., Bonadonna, C., and Watson, I. M.: Reconstructing the tephra dispersal pattern from the Bronze Age eruption of Santorini using an advection-diffusion model, *B. Volcanol.*, 74, 1485–1507, <https://doi.org/10.1007/s00445-012-0609-x>, 2012.
- Katrantsiotis, C., Kylander, M. E., Smittenberg, R. H., Yamoah, K. K. A., Hättstrand, M., Avramidis, P., Strandberg, N. A., and Norström, E.: Eastern Mediterranean hydroclimate reconstruction over the last 3600 years based on sedimentary n-alkanes, their carbon and hydrogen isotope composition and XRF data from the Gialova Lagoon, SW Greece, *Quaternary Sci. Rev.*, 194, 77–93, <https://doi.org/10.1016/j.quascirev.2018.07.008>, 2018.
- Katrantsiotis, C., Norström, E., Smittenberg, R. H., and Finne, M.: Climate changes in the Eastern Mediterranean over the last 5000 years and their links to the high-latitude atmospheric patterns and Asian monsoons, *Global Planet. Change*, 175, 36–51, <https://doi.org/10.1016/j.gloplacha.2019.02.001>, 2019.
- Keigwin, L. D.: The Little Ice Age and Medieval Warm Period in the Sargasso Sea, *Science*, 80, 1504–1508, <https://doi.org/10.1126/science.274.5292.1504>, 1996.
- Kelly, M. and Ó Grada, C.: The Waning of the Little Ice Age: Climate Change in Early Modern Europe, *J. Interdiscip. Hist.*, 44, 301–325, [https://doi.org/10.1162/JINH\\_a\\_00573](https://doi.org/10.1162/JINH_a_00573), 2014.
- Khamnueva-Wendt, S., Mitusov, A. V., Wendt, J., and Bork, H.-R.: Classification of buried soils, cultural, and colluvial deposits in the Viking town Hedeby, *Geoarchaeology*, 35, 313–337, <https://doi.org/10.1002/gea.21777>, 2019.
- Kiratzis, A., Sokos, E., Ganas, A., Tselentis, A., Benetatos, C., Roumelioti, Z., Serpentsidaki, A., Andriopoulos, G., Galanis, O., and Petrou, P.: The April 2007 earthquake swarm near Lake Trichonis and implications for active tectonics in western Greece, *Tectonophysics*, 452, 51–65, 2008.
- Koinig, K. A., Shoty, W., Lotter, A. F., Ohlendorf, C., and Sturm, M.: 9000 years of geochemical evolution of lithogenic major and trace elements in the sediment of an alpine lake – the role of climate, vegetation, and land-use history, *J. Paleolimnol.*, 30, 307–320, <https://doi.org/10.1023/A:1026080712312>, 2003.
- Köppen, W.: *Das geographische System der Klimate*, Gebrüder B., Berlin, Germany, 1936.

- Koussouris, T. S. and Diapoulis, A. C.: The aquatic vegetation of a large deep and oligotrophic lake (Lake Trichonis, western Greece), *Thalassographica*, 5, 33–40, 1982.
- Koutsodendris, A., Brauer, A., Zacharias, I., Putyrskaya, V., Klemm, E., Sangiorgi, F., and Pross, J.: Ecosystem response to human- and climate-induced environmental stress on an anoxic coastal lagoon (Etoliko, Greece) since 1930 AD, *J. Paleolimnol.*, 53, 255–270, <https://doi.org/10.1007/s10933-014-9823-1>, 2015.
- Koutsodendris, A., Brauer, A., Reed, J. M., Plessen, B., Friedrich, O., Hennrich, B., Zacharias, I., and Pross, J.: Climate variability in SE Europe since 1450 AD based on a varved sediment record from Etoliko Lagoon (Western Greece), *Quaternary Sci. Rev.*, 159, 63–76, 2017.
- Krüger, S. and Damrath, M.: In search of the Bølling-Oscillation: a new high resolution pollen record from the locus classicus Lake Bølling, Denmark, *Veg. Hist. Archaeobot.*, 29, 189–211, <https://doi.org/10.1007/s00334-019-00736-3>, 2020.
- Kylander, M. E., Ampel, L., Wohlfarth, B., and Veres, D.: High-resolution X-ray fluorescence core scanning analysis of Les Echets (France) sedimentary sequence: new insights from chemical proxies, *J. Quaternary Sci.*, 26, 109–117, <https://doi.org/10.1002/jqs.1438>, 2011.
- Luterbacher, J., García-Herrera, R., Akcer-On, S., Allan, R., Alvarez-Castro, M.-C., Benito, G., Booth, J., Büntgen, U., Cagatay, N., Colombaroli, D., Davis, B., Esper, J., Felis, T., Fleitmann, D., Frank, D., Gallego, D., Garcia-Bustamante, E., Glaser, R., Gonzalez-Rouco, F. J., Goosse, H., Kiefer, T., Macklin, M. G., Manning, S. W., Montagna, P., Newman, L., Power, M. J., Rath, V., Ribera, P., Riemann, D., Roberts, N., Sicre, M.-A., Silenzi, S., Tinner, W., Tzedakis, P. C., Valero-Garcés, B., van der Schrier, G., Vannière, B., Vogt, S., Wanner, H., Werner, J. P., Willett, G., Williams, M. H., Xoplaki, E., Zerefos, C. S., and Zorita, E.: A Review of 2000 Years of Paleoclimatic Evidence in the Mediterranean, in: *The Climate of the Mediterranean Region*, edited by: Lionello, P., Elsevier, 87–185, <https://doi.org/10.1016/C2011-0-06210-5>, 2012.
- Luterbacher, J., Werner, J. P., Smerdon, J. E. E., Fernández-Donado, L., González-Rouco, F. J. J., Barriopedro, D., Ljungqvist, F. C., Büntgen, U., Zorita, E., Wagner, S., Esper, J., McCarroll, D., Toreti, A., Frank, D., Jungclauss, J. H. H., Barriendos, M., Bertolin, C., Bothe, O., Brázdil, R., Camuffo, D., Dobrovolný, P., Gagen, M., García-Bustamante, E., Ge, Q., Gómez-Navarro, J. J. J., Guiot, J., Hao, Z., Hegerl, G. C. C., Holmgren, K., Klimentko, V. V. V., Martín-Chivelet, J., Pfister, C., Roberts, N., Schindler, A., Schurer, A., Solomina, O., Von Gunten, L., Wahl, E., Wanner, H., Wetter, O., Xoplaki, E., Yuan, N., Zanchettin, D., Zhang, H., and Zerefos, C.: European summer temperatures since Roman times, *Environ. Res. Lett.*, 11, 024001, <https://doi.org/10.1088/1748-9326/11/2/024001>, 2016.
- Magny, M., Joannin, S., Galop, D., Vannière, B., Haas, J. N., Bassetti, M., Bellintani, P., Scandolari, R., and Desmet, M.: Holocene palaeohydrological changes in the northern Mediterranean borderlands as reflected by the lake-level record of Lake Ledro, northeastern Italy, *Quaternary Res.*, 77, 382–396, <https://doi.org/10.1016/j.yqres.2012.01.005>, 2012.
- Mangini, A., Spötl, C., and Verdes, P.: Reconstruction of temperature in the Central Alps during the past 2000 yr from a  $\delta^{18}\text{O}$  stalagmite record, *Earth Planet. Sc. Lett.*, 235, 741–751, <https://doi.org/10.1016/j.epsl.2005.05.010>, 2005.
- Mann, M. E., Zhang, Z., Rutherford, S., Bradley, R. S., Hughes, M. K., Shindell, D., Ammann, C., Faluvegi, G., and Ni, F.: Global Signatures and Dynamical Origins of the Little Ice Age and Medieval Climate Anomaly, *Science*, 80, 1256–1260, <https://doi.org/10.1126/science.1177303>, 2009.
- McCormick, M., Büntgen, U., Cane, M. A., Cook, E. R., Harper, K., Huybers, P., Litt, T., Manning, S. W., Mayewski, P. A., More, A. F. M., Nicolussi, K., and Tegel, W.: Climate Change during and after the Roman Empire: Reconstructing the Past from Scientific and Historical Evidence, *J. Interdiscip. Hist.*, 43, 169–220, [https://doi.org/10.1162/JINH\\_a\\_00379](https://doi.org/10.1162/JINH_a_00379), 2012.
- Mercuri, A. M. and Sadori, L.: Mediterranean Culture and Climatic Change: Past Patterns and Future Trends, in: *The Mediterranean Sea: Its History and Present Challenges*, edited by: Goffredo, S. and Dubinsky, Z., Springer, Heidelberg, Germany, New York, USA, London, UK, 507–526, 2014.
- Meriam, E. O., Aurélie, H., Héléne, L., Volkan, K., Jacqueline, V. A., Gilles, L., Olivier, D., and Sabine, S.: Soil erosion in relation to land-use changes in the sediments of Amik Lake near Antioch antique city during the last 4 kyr, *Holocene*, 28, 104–118, <https://doi.org/10.1177/0959683617715702>, 2018.
- Meyers, P. A.: Applications of organic geochemistry to paleolimnological reconstructions: A summary of examples from the Laurentian Great Lakes, *Org. Geochem.*, 34, 261–289, [https://doi.org/10.1016/S0146-6380\(02\)00168-7](https://doi.org/10.1016/S0146-6380(02)00168-7), 2003.
- Mingram, J., Negendank, J. F. W., Brauer, A., Berger, D., Hendrich, A., Köhler, M., and Usinger, H.: Long cores from small lakes - Recovering up to 100 m-long lake sediment sequences with a high-precision rod-operated piston corer (Usinger-corer), *J. Paleolimnol.*, 37, 517–528, <https://doi.org/10.1007/s10933-006-9035-4>, 2007.
- Mook, W. G. and van der Plicht, J.: Reporting  $^{14}\text{C}$  activities and concentrations, *Radiocarbon*, 41, 227–239, <https://doi.org/10.1017/S0033822200057106>, 1999.
- Morellón, M., Anselmetti, F. S., Ariztegui, D., Brushliti, B., Sinopoli, G., Wagner, B., Sadori, L., Gilli, A., and Pambuku, A.: Human-climate interactions in the central Mediterranean region during the last millennia: The laminated record of Lake Butrint (Albania), *Quaternary Sci. Rev.*, 136, 134–152, <https://doi.org/10.1016/j.quascirev.2015.10.043>, 2016.
- Munsell, A. H.: *Munsell Soil Color Charts*, Munsell Color, Grand Rapids, Michigan, USA, 2000.
- Neukom, R., Steiger, N., Gómez-Navarro, J. J., Wang, J., and Werner, J. P.: No evidence for globally coherent warm and cold periods over the preindustrial Common Era, *Nature*, 571, 550–554, <https://doi.org/10.1038/s41586-019-1401-2>, 2019.
- Nieto-Moreno, V., Martínez-Ruiz, F., Giral, S., Jiménez-Espejo, F., Gallego-Torres, D., Rodrigo-Gámiz, M., García-Orellana, J., Ortega-Huertas, M., and de Lange, G. J.: Tracking climate variability in the western Mediterranean during the Late Holocene: a multiproxy approach, *Clim. Past*, 7, 1395–1414, <https://doi.org/10.5194/cp-7-1395-2011>, 2011.
- Norström, E., Katrantsiotis, C., Finné, M., Risberg, J., Smittenberg, R. H., and Bjursäter, S.: Biomarker hydrogen isotope composition ( $\delta\text{D}$ ) as proxy for Holocene hydroclimatic change and seismic activity in SW Peloponnese, Greece, *J. Quaternary Sci.*, 33, 563–574, <https://doi.org/10.1002/jqs.3036>, 2018.

- Olsen, J., Anderson, N. J., and Knudsen, M. F.: Variability of the North Atlantic Oscillation over the past 5,200 years, *Nat. Geosci.*, 5, 808–812, <https://doi.org/10.1038/ngeo1589>, 2012.
- Overbeck, J., Anagnostidis, K., and Economou-Amilli, A.: A limnological survey of three Greek lakes: Trichonis, Lyssimachia and Amvrakia, *Arch. Hydrobiol.*, 95, 365–394, 1982.
- Papadopoulos, G. A. and Plessa, A.: Magnitude–distance relations for earthquake-induced landslides in Greece, *Eng. Geol.*, 58, 377–386, [https://doi.org/10.1016/S0013-7952\(00\)00043-0](https://doi.org/10.1016/S0013-7952(00)00043-0), 2000.
- Papadopoulos, G. A., Baskoutas, I., and Fokaefs, A.: Historical seismicity of the Kyparissiakos Gulf, western Peloponnese, Greece, *Boll. Geof. Teor. Appl.*, 55, 389–404, <https://doi.org/10.4430/bgta0096>, 2014.
- Papapostolou, I. A.: Early Thermos. New Excavations 1992–2003, The Archaeological Society at Athens, X, Athens, Greece, 248 pp., 2012.
- Psomiadis, D., Dotsika, E., Albanakis, K., Ghaleb, B., and Hillaire-Marcel, C.: Speleothem record of climatic changes in the northern Aegean region (Greece) from the Bronze Age to the collapse of the Roman Empire, *Palaeogeogr. Palaeoclimatol.*, 489, 272–283, <https://doi.org/10.1016/j.palaeo.2017.10.021>, 2018.
- R Core Team: R: A language and environment for statistical computing, R Foundation for Statistical Computing, Vienna, Austria, Austria, available at: <https://www.r-project.org/> (last access: 30 June 2020), 2019.
- Reimer, P. J., Bard, E., Bayliss, A., Beck, J. W., Blackwell, P. G., Ramsey, C. B., Buck, C. E., Cheng, H., Edwards, R. L., Friedrich, M., Grootes, P. M., Guilderson, T. P., Hafflidason, H., Hajdas, I., Hatte, C., Heaton, T. J., Hoffmann, D. L., Hogg, A. G., Hughen, K. A., Kaiser, K. F., Kromer, B., Manning, S. W., Niu, M., Reimer, R. W., Richards, D. A., Scott, E. M., Southon, J. R., Staff, R. A., Turney, C. S. M., and van der Plicht, J.: IntCal13 and Marine13 radiocarbon age calibration curves 0–50 000 Years cal BP, *Radiocarbon* 55, 1869–1887, [https://doi.org/10.2458/azu\\_js\\_rc.55.16947](https://doi.org/10.2458/azu_js_rc.55.16947), 2013.
- Roberts, N., Eastwood, W. J., Kuzucuoglu, C., Fiorentino, G., and Caracuta, V.: Climatic, vegetation and cultural change in the eastern Mediterranean during the mid-Holocene environmental transition, *Holocene*, 21, 147–162, <https://doi.org/10.1177/0959683610386819>, 2011.
- Roberts, N., Moreno, A., Valero-Garcés, B. L., Corella, J. P., Jones, M., Allcock, S., Woodbridge, J., Morellón, M., Luterbacher, J., Xoplaki, E., and Türkeş, M.: Palaeolimnological evidence for an east-west climate see-saw in the Mediterranean since AD 900, *Global Planet. Change*, 84–85, 23–34, <https://doi.org/10.1016/j.gloplacha.2011.11.002>, 2012.
- Sabatier, P., Wilhelm, B., Ficetola, G. F., Moiroux, F., Poulencard, J., Develle, A.-L., Bichet, A., Chen, W., Pignol, C., Reyss, J.-L., Gielly, L., Bajard, M., Perrette, Y., Malet, E., Taberlet, P., and Arnaud, F.: 6-kyr record of flood frequency and intensity in the western Mediterranean Alps – Interplay of solar and temperature forcing, *Quaternary Sci. Rev.*, 170, 121–135, <https://doi.org/10.1016/j.quascirev.2017.06.019>, 2017.
- Seguin, J., Bintliff, J. L., Grootes, P. M., Bauersachs, T., Dörfler, W., Heymann, C., Manning, S. W., Müller, S., Nadeau, M.-J., Nelle, O., Steier, P., Weber, J., Wild, E.-M., Zagana, E., and Unkel, I.: 2500 years of anthropogenic and climatic landscape transformation in the Stymphalia polje, Greece, *Quaternary Sci. Rev.*, 213, 133–154, <https://doi.org/10.1016/j.quascirev.2019.04.028>, 2019.
- Seguin, J., Avramidis, P., Haug, A., Kessler, T., Schimmelmann, A., and Unkel, I.: Reconstruction of palaeoenvironmental variability based on an inter-comparison of four lacustrine archives on the Peloponnese (Greece) for the last 5000 years, in review, 2020a.
- Seguin, J., Avramidis, P., Dörfler, W., Emmanouilidis, A., and Unkel, I.: Geochemical and sedimentological record of sediment core TR11 retrieved from Lake Trichonida (southern Greece), *PANGAEA*, <https://doi.org/10.1594/PANGAEA.921324>, 2020b.
- Spearman, C.: The Proof and Measurement of Association between Two Things, *Am. J. Psychol.*, 15, 72–101, <https://doi.org/10.2307/1412159>, 1904.
- Statham, P. J., Homoky, W. B., Parker, E. R., Klar, J. K., Silburn, B., Poulton, S. W., Kröger, S., Pearce, R. B., and Harris, E. L.: Extending the applications of sediment profile imaging to geochemical interpretations using colour, *Cont. Shelf Res.*, 185, 16–22, <https://doi.org/10.1016/j.csr.2017.12.001>, 2017.
- Tafas, T. and Economou-Amilli, A.: Limnological survey of the warm monomictic lake Trichonis (central western Greece). II. Seasonal phytoplankton periodicity – a community approach, *Hydrobiologia*, 344, 141–153, <https://doi.org/10.1023/A:1002962513146>, 1997.
- Tafas, T., Danielidis, D., Overbeck, J., and Economou-Amilli, A.: Limnological survey of the warm monomictic lake Trichonis (central western Greece). I. The physical and chemical environment, *Hydrobiologia*, 344, 129–139, <https://doi.org/10.1023/A:1002914629984>, 1997.
- Taymaz, T., Yilmaz, Y., and Dilek, Y.: The geodynamics of the Aegean and Anatolia: introduction. *Geol. Soc. London, Spec. Publ.* 291, 1–16, <https://doi.org/10.1144/SP291.1>, 2007.
- Tjallingii, R., Röhl, U., Kölling, M., and Bickert, T.: Influence of the water content on X-ray fluorescence corescanning measurements in soft marine sediments, *Geochem. Geophys. Geosyst.*, 8, 1–12, <https://doi.org/10.1029/2006GC001393>, 2007.
- Unkel, I., Schimmelmann, A., Shriner, C., Forsén, J., Heymann, C., and Brückner, H.: The environmental history of the last 6500 years in the Asea Valley (Peloponnese, Greece) and its linkage to the local archaeological record, *Z. Geomorphol. Suppl.*, 58, 89–107, <https://doi.org/10.1127/0372-8854/2014/S-00160>, 2014.
- Vaezi, A., Ghazban, F., Tavakoli, V., Routh, J., Beni, A. N., Bianchi, T. S., Curtis, J. H., and Kylin, H.: A Late Pleistocene–Holocene multi-proxy record of climate variability in the Jazmurian playa, southeastern Iran, *Palaeogeogr. Palaeoclimatol.*, 514, 754–767, <https://doi.org/10.1016/j.palaeo.2018.09.026>, 2019.
- Walsh, K., Berger, J.-F., Roberts, C. N., Vanniere, B., Ghilardi, M., Brown, A. G., Woodbridge, J., Lespez, L., Estrany, J., Glais, A., Palmisano, A., Finné, M., and Verstraeten, G.: Holocene demographic fluctuations, climate and erosion in the Mediterranean: A meta data-analysis, *Holocene*, 29, 864–885, <https://doi.org/10.1177/0959683619826637>, 2019.
- Warken, S. F., Fohlmeister, J., Schröder-Ritzrau, A., Constantin, S., Spötl, C., Gerdes, A., Esper, J., Frank, N., Arps, J., Terente, M., Riechelmann, D. F. C., Mangini, A., and Scholz, D.: Reconstruction of late Holocene autumn/winter precipitation variability in SW Romania from a high-resolution speleothem trace element record, *Earth Planet. Sc. Lett.*, 499, 122–133, <https://doi.org/10.1016/j.epsl.2018.07.027>, 2018.

